THESIS

ESTIMATING PRE-FIRE FOREST STRUCTURE WITH STEREO IMAGERY AND POST-FIRE LIDAR

Submitted by

Steven Filippelli

Graduate Degree Program in Ecology

In partial fulfillment of the requirements

For the Degree of Master of Science

Colorado State University

Fort Collins, Colorado

Summer 2016

Master's Committee

Advisor: Michael Lefsky

Monique Rocca
Jason Sibold

ABSTRACT

ESTIMATING PRE-FIRE FOREST STRUCTURE WITH STEREO IMAGERY AND POST-FIRE LIDAR

Lidar has become an established tool for mapping forest structure attributes including those used as inputs for fire behavior and effects modelling. However, lidar is rarely available to document pre-fire conditions due to its sparse availability. In contrast, aerial imagery is regularly collected in many regions, and advances in stereo image matching have enabled the creation of dense photogrammetric point clouds similar to those from lidar. As part of a study of the physical and ecological impacts of the 2012 High Park Fire, we generated a photogrammetric point cloud from pre-fire aerial imagery collected in 2008 and calculated forest height using a digital terrain model generated from a 2013 post-fire lidar collection. A suite of canopy height and density metrics were created from both the pre-fire photogrammetry and the post-fire lidar point clouds. These metrics were compared to each other and to forest structure attributes measured in the field.

For unburned areas, we found strong relationships between corresponding lidar and photogrammetry height and density metrics with biases that were consistent with known differences in each sensor's method of sampling the canopy. Regressions models of field-measured forest structure attributes incorporating both lidar and photo metrics demonstrated that a single equation could estimate some forest structure attributes without significant intercept or slope bias due to the source of the metrics (i.e. photo or lidar). Models of aboveground biomass on unburned plots had similar root mean square errors for lidar (29.3%), photogrammetry (31.0%), and combined data sources (RMSE = 29.1% and source intercept bias = 34.64 Mg ha^{-1} and slope bias = -0.28). Similar results were obtained for Lorey's height, basal area, and canopy bulk density. Models of structure in burned areas derived from post-fire lidar had lower performance than photogrammetry due to the fire's consumption of

canopy materials which generally reduced the explanatory power of lidar density metrics. Pre-fire forest structure information could aid assessments of contributing factors such as canopy fuels and fire effects such as loss of biomass. The wide spatial and temporal coverage of aerial photos and growing coverage of lidar could enable many other applications of combining photogrammetry with lidar, including assessments of changes in forest carbon storage.

ACKNOWLEDGEMENTS

Thank you Miranda Middleton for regularly dragging me away from my computer and into the mountains so I could be reminded of why I chose to pursue a degree in ecology. I also want to thank my parents, Doreen Godfrey and Frank Filippelli, and grandfather, Guy Filippelli, for their constant support and for their financial assistance earlier in my life, which has enabled me to pursue a fulfilling albeit not very lucrative career in ecology and remote sensing.

The help I received from friends and colleagues along with our conversations was the most enjoyable aspect to pursuing my degree. In particular, my work would not be possible without the contributions of Brandon Stone, and I also benefited greatly from the help and support of Monique Rocca, Aniruddha Ghosh, David Gwenzi, Micah Wright, Jason Sibold, Tony Vorster, Aaron Sidder, Adam Johnson, Codie Wilson, and many others. Thank you especially to my advisor, Michael Lefsky, who deserves much of the credit for this work.

TABLE OF CONTENTS

1 Introduction

Remote sensing has matured to the point that it is now relied on for wall-to-wall mapping of forest structure for carbon accounting, operational forestry, fuels management, conservation biology, and numerous other applications. While two-dimensional optical remote sensing systems are sometimes used for these applications, sensors and methods which are capable of detecting three-dimensional structure (e.g. interferometric synthetic aperture radar, light detection and ranging (lidar), and stereo photogrammetry) generally provide more accurate estimates of forest structure attributes. Lidar in particular has gained widespread adoption in forest research and management applications over the last two decades because of its ability to accurately estimate the vertical structure of forest canopies. By sampling the ground topography in addition to the canopy, lidar is capable of directly estimating canopy height. Canopy height and cover metrics derived from lidar greatly enhance prediction accuracy in models of basal area, timber volume, leaf area index, aboveground biomass, canopy bulk density, and other structure attributes.

This ability has made lidar appealing to numerous land management and research organizations. For example, lidar is now widely used for operational forest inventories in Norway, Finland, Canada, and other parts of the world (Maltamo, Næsset, & Vauhkonen, 2014). Recent research has focused on implementing lidar for national-scale carbon accounting that meets the measuring, reporting, and verification standards of carbon monitoring programs such as the Reducing Emissions from Deforestation and forest Degradation framework developed by the United Nations (Goetz & Dubayah, 2011). Canopy fuels maps required for fire behavior modeling have been derived from various passive and active remote sensing systems, but lidar is often the most effective of these technologies due to its ability to sample the vertical distribution of the entire canopy (Keane, 2015). By capturing the three-dimensional structure of vegetation, lidar has also proven effective at mapping key habitat characteristics for wildlife research (e.g. Vierling, Vierling, Gould, Martinuzzi, & Clawges, 2008). Dubayah

and Drake (2000) and Lefsky, Cohen, Parker and Harding (2002), among others, recognized the potential for lidar in these and other applications during its early development which spurred lidar's rapid and widespread adoption.

Disturbance has long been recognized as an essential process in forest ecosystems, and remotely sensed imagery is frequently used to evaluate the effects of forest disturbances (Frolking et al., 2009; Lentile, Holden, et al., 2006). Despite its rapid growth, applications of lidar for understanding forest disturbance remain limited because pre-disturbance lidar is rarely available. Several studies have demonstrated the potential of lidar for measuring canopy fuels that serve as input to fire behavior models (Andersen, McGaughey, & Reutebuch, 2005; Erdody & Moskal, 2010; Hermosilla, Ruiz, Kazakova, Coops, & Moskal, 2014), but only a few studies have collected lidar data after a fire to investigate the potential causes and effects of the fire. Lefsky, Turner, Guzy, and Cohen (2005) estimated net primary productivity following stand initiation from disturbances such as fire and logging using biomass estimates from lidar and stand age estimated from Landsat change detection. Wulder et al. (2009) used pre- and post-fire profiling lidar and Landsat imagery to study the relationship between forest structure and post-fire conditions. Goetz, Sun, Baccini, and Beck (2010) evaluated changes in canopy height and vegetation regrowth following fires in Alaska with the Geoscience Laser Altimeter System, a spaceborne waveform lidar sensor. Kane et al. (2013) used lidar to gauge the effect of burn severity on canopy structure in Yosemite National Park and found that increased severity was related to greater canopy openness and patchiness even decades after a fire. Two forest service technical reports have demonstrated the potential for using pre- and post-fire lidar to characterize changes in vegetation from disturbance (Kaufmann, Stoker, & Greenlee, 2006; R. A. White & Dietterick, 2012).

It may also be possible to obtain pre-fire canopy height information from airborne lidar collected immediately after a fire by observing the remaining burned snags which might allow estimation of pre-fire forest structure. This type of analysis is complicated by the challenge of obtaining

lidar returns from the canopy of burned stands. Charred and leafless trees have low surface area and reflectivity which reduces their likelihood of being detected and accurately measured by a lidar sensor. Adequately measuring the height of burned snags may require higher laser power and pulse density than what is typically necessary for mapping unburned forests. Wing, Eklund, and Sessions (2010) is the only study to date to assess the accuracy of lidar for measuring individual burned trees. Using lidar with point densities between 1.6 and 2.5 points per m^2 they achieved height accuracies of 2.8-4 m (RMSE) and an omission error of 15%. Their results suggest that lidar could still serve as a useful tool for forest inventory in a post-fire landscape, but to our knowledge, no studies have examined the effect of burn severity on lidar height and density metrics and how it might impact estimates of pre-fire forest structure.

In recent years photogrammetry has reemerged as a possible alternative to lidar because of improvements in image matching algorithms, increased computational power, and low cost aerial image collection, including the rapid growth of unmanned aerial systems (Colomina & Molina, 2014). Modern image matching algorithms such as Semiglobal Matching (Hirschmuller, 2008) are capable of producing point clouds with a higher density than lidar at lower cost, but the photogrammetric point cloud only captures the canopy surface as opposed to the full distribution of observed surfaces such as those obtained from multiple-return or waveform lidar. Since image matching in forests often results in sparse points on the terrain surface, a high resolution digital terrain model (DTM) must be obtained from lidar (or another technology capable of penetrating the canopy) to normalize the photogrammetric point cloud to ground level. Height and density metrics derived from the normalized photogrammetric point cloud have proven effective at estimating forest structure attributes but with a slightly lower accuracy than lidar (J. C. White et al., 2013). To date, almost all studies using photogrammetric point clouds have taken place in boreal forests (Bohlin, Wallerman, & Fransson, 2012; Gobakken, Bollandsås, & Næsset, 2015; Järnstedt et al., 2012; Montesano, Sun, Dubayah, & Ranson, 2014; Nurminen, Karjalainen, Yu,

Hyyppä, & Honkavaara, 2013; Pitt, Woods, & Penner, 2014; Vastaranta et al., 2013), and there is a need to test this approach in other forest types. Existing research has also emphasized the application of this approach to updating forest inventories by combining a pre-existing lidar DTM with new stereo imagery (J. C. White et al., 2013), but the combination of lidar and photogrammetry can also be used to examine past landscape states by collecting airborne lidar in locations that have pre-existing stereo imagery (Véga & St-Onge, 2008). Successful application of this approach in other forest types could enable estimates of forest structure within any several year time window for many parts of the United States because of the widespread and frequent collection of aerial and satellite imagery with stereo overlap.

Mapping past forest structure conditions with lidar or photogrammetry has potential applications in quantifying changes in structure and understanding the influence of pre-fire structure on fire effects and post-fire trajectories. Field studies have incorporated plot-level measures of pre-fire structure in models of burn severity to compare its influence relative to topography and weather (Alexander, Seavy, Ralph, & Hogoboom, 2006; Lydersen, North, & Collins, 2014; Turner, Romme, & Gardner, 1999). Wall-to-wall maps of pre-fire structure derived from imagery or mixed-source spatial databases have also been used for this purpose (Bigler, Kulakowski, & Veblen, 2005; Lentile, Smith, & Shepperd, 2006; Odion et al., 2004; Thompson & Spies, 2009), but only recently has remotely sensed three-dimensional structure been incorporated in modelling burn severity (Kane et al., 2015). Pre-fire basal area and tree density have been included in models of post-fire tree regeneration (Broncano & Retana, 2004; Greene & Johnson, 1999; Harvey, Donato, Romme, & Turner, 2013). Mapping these pre-fire structure attributes could be used to estimate seedling density across a burn area and forecast post-fire succession trajectories. Pre-fire structure has also be used to estimate post-fire habitat quality for wildlife such as woodpeckers (Nappi & Drapeau, 2011). These applications illustrate the utility of mapping pre-fire structure with remote sensing to enable spatial analysis of disturbance effects and post-disturbance trajectories.

This study compares the potential of pre-fire photogrammetry (with a post-fire DTM from lidar) and post-fire lidar for mapping pre-fire forest structure. The study area covers the High Park fire which took place in northern Colorado in 2012. We compare lidar and photogrammetry estimates of forest structure attributes in unburned areas to examine whether these two remote sensing methods can be used interchangeably. If so, photogrammetry could serve as an alternative to lidar for mapping structure of similar forests, and direct comparison of estimates from lidar and photogrammetry could characterize change in forest structure. We also evaluate the relative effectiveness of using post-fire lidar and pre-fire photogrammetry for recovering pre-fire forest structure in burned areas. We expect high levels of canopy consumption to cause inconsistent decreases in canopy height and density metrics from post-fire lidar, which will lead to a weaker relationship with associated forest structure attributes. To test this, we compare estimates of pre-fire forest structure made with post-fire lidar to estimates made with pre-fire photogrammetry. To evaluate the effect of fire on the quality of statistical models of forest attributes, we compared models of forest attributes from lidar in burned and unburned areas. Maps of pre-fire forest structure are derived from the most accurate models and used to evaluate the influence of canopy fuels on burn severity and also evaluate the effects of the fire on forest structure such as loss of biomass.

2 Methods

2.1 Study area

Field and remotely sensed data were collected within and immediately surrounding the burn perimeter of the High Park fire in northern Colorado (40°37'N, 105°21'W) (Figure 1). The High Park fire burned an area of approximately 35,300 hectares in June 2012, half of which was composed of public lands (Natural Resources Conservation Service, Larimer County, United States Forest Service, & Colorado Department of Transportation, 2012). Burn severity was heterogeneous over the entire study area, with 12.8%, 27.5%, 18.7%, and 41% of the area consisting of unburned, low, moderate, and high burn severity, respectively (Stone, 2015). Elevation ranges from 1600 m in the eastern foothills immediately outside the burn perimeter to 3100 m in the more mountainous western region of the burn area. Lower elevations are primarily composed of mature montane coniferous forests dominated by a mixture of ponderosa pine (*Pinus ponderosa*) and Douglas-fir (*Psuedotsuga menziesii*) on northern aspects and open ponderosa pine stands on southern aspects. Higher elevations in the western portion of the study area are dominated by mature lodgepole pine (*Pinus contorta*) stands. Aspen stands, grasslands, shrublands, and riparian areas comprise a much smaller proportion of the total area. Immediately prior to the fire, approximately 17% of the burn area contained pines in the red or grey phase of mountain pine beetle (*Dendroctonus ponderosae*) attack which began to reach epidemic levels in 2009 (Stone, 2015).

2.2 Field data

Field data collected in the fall of 2012 were used to estimate forest structure attributes for 50 unburned and 45 burned inventory plots. Plot locations were randomly distributed according to a spatially clustered plot design stratified by forest type, elevation, prior beetle activity, and burn severity. Plot centers were georeferenced with Trimble Juno or GeoXH GPS receivers and differentially corrected using a nearby continuously operating reference station (CORS) to an average horizontal precision of 3.1

m. Inventory plots were 20 m by 20 m with 10 m by 10 m sub-plots. Tree measurements in all sub-plots included species, diameter at breast height (DBH), stem location, burn status, and mortality status for all trees with a DBH greater than 10 cm. For all trees with burn signs, such as charred bark, needle loss, or scorch, we recorded the scorch height and we visually estimated crown consumption as the percentage of the pre-fire crown volume consumed by the fire. Tree heights were measured with a laser hypsometer for at least 10 trees and the tallest tree in each 20 m by 20 m plot beginning in the southwest sub-plot and sampling other sub-plots if necessary.

Tree height was estimated for the unmeasured trees on each plot using the R package 'lmfor' (Mehtatalo, 2015) to implement species-specific nonlinear mixed-effects models using the Wykoff height-diameter function (Wykoff, Crookston, & Stage, 1982). Unburned and undamaged trees were used as a source of heights, and species with fewer than 10 measured trees had heights estimated using the Wykoff model with coefficients from the Forest Vegetation Simulator Central Rockies variant (Keyser & Dixon, 2015). Estimated heights were also used for burned trees which had their height reduced due to lean or breakage so that estimates of mean height and Lorey's height (i.e. mean basal area weighted height) on burned plots would more accurately reflect their pre-fire status. Root mean square errors of tree height imputation were less than 2 m or 18% of the mean observed height for all species, which we deemed acceptable for estimation of mean height and Lorey's height. Even though field data were collected four years after the aerial imagery and one year prior to the lidar, similar studies have assumed that the slow growth rate of these mature pine and mixed conifer forests makes tree size corrections unnecessary (Hall, Burke, Box, Kaufmann, & Stoker, 2005).

Forest structure attributes derived from field data included maximum canopy height, Lorey's height, aboveground biomass, basal area, canopy bulk density, and canopy base height (Table 1). We chose to include maximum canopy height because it is the attribute most directly measured by lidar and photogrammetry. Therefore it serves as an indicator of the height measurement accuracy of each

method without requiring assumptions about how it samples the canopy, as would be necessary for more complex tree height indices (e.g. the mean height of dominant and co-dominant trees). For lodgepole pine we calculated aboveground biomass from allometries developed by Pearson, Fahey, and Knight (1984) in the nearby Medicine Bow Mountains; aboveground biomass for all other species was calculated from the appropriate general equations developed by Chojnacky, Heath, and Jenkins (2014). The Chojnacky et al. (2014) allometries, which are an update to the meta-analysis of individual species allometries in North America performed by Jenkins, Chojnacky, Heath, and Birdsey (2003), contains 35 new general equations which divide species on the basis of taxonomic grouping and wood specific gravity. In the burned areas, tree boles were rarely charred deeply enough to affect diameter measurements, even for beetle-killed trees in severely burned plots, so no correction was applied to pre-fire DBH measurements. This method of pre-fire stand reconstruction has been implemented in other studies for carbon accounting (Johnson et al., 2005; Meigs, Donato, Campbell, Martin, & Law, 2009; Michalek, French, Kasischke, Johnson, & Colwell, 2000). Pre-fire canopy bulk density and canopy base height were estimated for plots which had ponderosa pine, lodgepole pine, or Douglas-fir as the dominant species. These estimates were based on allometric equations that consider dominant species, stand density, basal area, and mean canopy height using the appropriate equations from Cruz, Alexander, and Wakimoto (2003).

2.3 Remote sensing data collection and processing

NEON's Airborne Observatory Platform collected small footprint discrete return lidar over the entire burn scar and surrounding area in July 2013 using an Optech ALTM Gemini. Ninety-seven flight lines with ~30% overlap were collected over the burn area using a mean swath pulse density of 1.87 pulses per square meter, and were delivered as up to four discrete returns in LAS format (Table 2). Initial processing involved identification of ground points with LAStools (Isenburg, 2011) which uses a progressive TIN densification algorithm similar to the method developed by Axelsson (2000). The ground

points and resulting DTM were used to calculate the height of points above the ground surface. Three categories of point cloud metrics were calculated from all points that were greater than 2 m above the terrain (Table 3). Height profile metrics were calculated using all point returns above the 2 m cutoff and included the height minimum, maximum, mean, quadratic mean, and six height percentiles. The height variation category included the standard deviation, coefficient of variation, skew, kurtosis, range, and interquartile range of point heights. The point density category included canopy cover (percent of first returns above the 2 m cutoff), canopy density (percent of all returns above the 2 m cutoff), and the percent of all returns within four fixed height intervals.

Aerial images were collected in 2008 using a Z/I Imaging DMC-1 camera in 15 flight lines at an altitude of 3200 m above ground level with approximately 60% forward overlap and 30% side overlap, which enables stereo photogrammetric processing (Table 2). The images have four bands (red, green, blue, and near infrared) with ~1.2 m ground sampling distance (GSD) and a higher resolution panchromatic band that was used to pan-sharpen the images to ~30 cm GSD. Initial camera locations and orientation obtained from the aircraft's GPS and inertial measurement unit were corrected in a bundle block adjustment with 40 control points identified on a lidar intensity image and DTM to co-register the images to the lidar data. Coregistration with the lidar had a horizontal RMSE of 0.72 m and a vertical RMSE of 0.82 m as determined from 9 check points which were also derived from the lidar intensity image and DTM. Stereo image matching in the PhotoScan software (*Photoscan Professional Edition*, 2015) with the "Ultra Quality" setting produced a photogrammetric point cloud capturing the canopy surface with an average point density of 12.91 points per square meter over plot areas and 15.89 points per square meter for the entire study area. The lidar DTM was subtracted from the photogrammetric point cloud to calculate the height of points above the ground surface. We then calculated the same point cloud metrics as done for the lidar (Table 3).

The images were orthorectified with the lidar DTM to a spatial resolution of 0.25 m and mosaicked for producing vegetation and image texture metrics (Table 3). Vegetation and texture indices represent a source of potentially useful information which are not commonly available for lidar-based modelling of forest structure but can easily be produced from aerial imagery. From the orthomosaic we calculated the Normalized Difference Vegetation Index (NDVI), which is associated with the quantity of healthy foliage and related attributes (Carlson & Ripley, 1997). Since the imagery was mostly collected in the summer of 2008, NDVI should be related to the amount of live vegetation prior to the bark beetle infestation which began to reach red-phase at epidemic levels in our study area starting in 2009 (Stone, 2015). First-order texture indices (e.g. variance of pixels in a moving window) and second-order indices (e.g. contrast of a grey-level co-occurrence matrix) were calculated from NDVI. These indices have been associated with vegetation structure in other studies (Hudak & Wessman, 1998; Tuominen & Pekkarinen, 2005) and may provide additional explanatory power over point-cloud based height and cover metrics derived from photogrammetry. A grey level co-occurrence matrix was calculated for each pixel falling within the plot area from the NDVI of the aerial imagery using a 3 by 3 window, a shift of one in the x and y direction and 64 quantization levels. Second-order texture indices, also known as Haralick texture features (Haralick, Shanmugam, & Dinstein, 1973), were calculated from the grey level co-occurrence matrix for every pixel falling within the plot area, and the average value of each index was used as the texture metric for the plot (Table 3). We examined the relationship between these indices and forest structure, and included them in regression modelling to evaluate whether they could improve model performance.

2.4 Data analysis

2.4.1 Effect of crown consumption on post-fire lidar

We examined the effects of burn severity on post-fire lidar metrics and their ability to estimate pre-fire forest structure through three analyses. Scatterplots and linear models were used to identify the

effect of canopy consumption on lidar metrics and on their ability to estimate pre-fire forest height and tree density attributes. We compared maximum lidar point height ($Hmax_{lidar}$) to maximum tree height measured in the field since they should have the most direct correspondence. Estimates of canopy cover are often critical for estimating forest structure attributes such as aboveground biomass from lidar because cover is related to stand density. Since field data was collected after the fire, it was not possible to obtain field measurements of pre-fire canopy cover on burned plots for comparison to the post-fire lidar estimates of cover. NDVI from May 2012 RapidEye imagery was weakly correlated (r = 0.32) with lidar estimates of canopy cover in forested unburned areas, which indicated that pre-fire NDVI may be a poor measure of canopy cover in this case. Instead, we selected field-measured stem density as a proxy for pre-fire cover to assess the influence of canopy consumption on post-fire lidar cover metrics because cover and the square root of stand density in unburned plots are highly correlated. Scatterplots of these two relationships (maximum tree height ~ *Hmax* and tree density ~ *cover*) and associated linear models indicate how sensitive lidar measurements were to canopy consumption.

We also examined the effect of burn severity on post-fire lidar metrics and their association with forest structure attributes through multiple regression models which incorporated estimates of canopy consumption as an explanatory variable. The percentage of each tree's crown volume which was consumed by the fire was visually estimated in the field. The average of these tree-level crown consumption estimates (*AvgCC*) was included as a single variable and as an interaction term with the selected lidar metrics. We tested the significance of these interactions and compared the percent of variance explained with and without their inclusion.

2.4.2 Comparison of lidar and photogrammetric point clouds

Metrics derived from the distribution of lidar point heights or the proportion of points within vertical layers are often excellent predictors of forest structure attributes such as aboveground biomass. These metrics can also be calculated from photogrammetric point clouds, but the physical meaning of

photogrammetry-based metrics do not have a one-to-one correspondence with lidar-based metrics because photogrammetry only samples the outer surface of the canopy whereas lidar can sample both the surface and interior of the canopy by penetrating through gaps between individual leaves and branches. As such, lidar can accurately estimate canopy cover (Korhonen, Korpela, Heiskanen, & Maltamo, 2011) and the vertical distribution of all canopy elements (Figure 2). To examine the magnitude of difference between these two remote sensing approaches, we used scatterplots and linear models to compare corresponding height and density metrics derived from the lidar and photogrammetric point clouds. Strong correlations between corresponding metrics generated from each point cloud, along with slopes near to one and intercepts near to zero, would indicate that those metrics are relatively insensitive to the presence of canopy interior points. The lack of an identity relationship would indicate that lidar and photogrammetric estimates could not be used interchangeably in regression equations. However, the metrics derived from photogrammetry (or lidar) needn't be less informative predictors of forest structure on their own. In some previous studies, height metrics derived solely from lidar first returns were selected as more informative predictors than metrics derived from all returns (e.g. Hall et al., 2005; Næsset, 2002), which indicates that in some cases information on the canopy surface alone can be more strongly related to forest structure attributes. We also examined the correlation between the metrics from each sensor and several forest structure attributes to understand how differences between lidar and photogrammetry metrics affected their association with forest structure.

2.4.3 Estimates of forest structure attributes from lidar and photogrammetry

We used ordinary least squares regression models to compare the ability of canopy metrics derived from lidar and photogrammetry point clouds to estimate forest structure attributes. Analyses were performed separately for burned and unburned plots. Results for unburned plots can be used to address questions related to the relative performance of lidar and photogrammetry for future studies of

temperate coniferous forest structure. Analyses for burned plots allow us to compare the relative utility of using post-fire lidar and pre-fire photogrammetry for estimating pre-fire forest structure. In addition, the utility of image texture and vegetation metrics was examined by comparing models of forest structure attributes created from photogrammetric point cloud metrics with and without these image metrics.

While these analyses inform our understanding of how the two sets of metrics perform for estimating forest structure, direct comparison of models is hampered by collinearity of the independent variables which makes it difficult to evaluate differences in variable selection. For instance, models based on either lidar or photogrammetry data sources might select different independent variables, but those independent variables might be highly correlated in both datasets. To address this problem, we combined the observed point cloud metrics from lidar and photogrammetry and duplicated the observed forest structure attribute for variable selection and regression modelling of unburned plots. We then regressed the predictions from these models on the observed values and included the data source as a categorical variable to test if data from lidar or photogrammetry could be used interchangeably in the same model without significant bias.

To select a subset of independent variables to use in each regression model, we examined correlations of individual point cloud and image metrics with forest structure attributes. A correlation-based filtering strategy was first employed to select one independent variable from each of the five variable classes: height, height variability, density, texture, and vegetation indices (Table 3). Within each class, the variable which had the highest correlation with the response was kept in the regression model. Final models were selected by identifying the subset of the filtered variables which yielded the lowest Akaike Information Criterion (AIC) with a condition number less than 30. This method of variable selection yielded parsimonious models and reduced potential problems with multicollinearity in the final model since variables were highly correlated within the categories but not between them. We

compared the model fit for the different attributes and scenarios by the adjusted coefficient of determination (Adj R^2). Model prediction accuracy was compared by the root mean square error from leave-one-out cross-validation expressed as a percent of the mean observed value (%RMSE). Model selection was performed within a cross-validation loop to avoid overestimating prediction accuracy (Kuhn & Johnson, 2013).

3 Results

3.1 Effect of crown consumption on post-fire lidar

High canopy consumption weakened the relationship between lidar cover metrics and pre-fire forest structure attributes, but had little effect on lidar's ability to estimate pre-fire canopy height. Contrary to our expectations, pre-fire maximum tree height was noticeably underestimated by lidar on only a few of the severely burned plots, and the correlation between observed maximum tree height and $Hmax_{lidar}$ was similar for burned and unburned plots (Figure 3). By contrast, the relationship between $cover_{lidar}$ and pre-fire tree density was much weaker in burned plots (Figure *4*) because severely burned plots often had a $cover_{lidar}$ near zero even when pre-fire tree density was relatively high. Since the imagery was collected before the fire, high canopy consumption did not decrease the strength of the relationship between $Hmax_{photo}$ and pre-fire maximum tree height or $cover_{photo}$ and pre-fire tree density. In fact, the relationship between $cover_{photo}$ and tree density was weaker on unburned plots than burned plots primarily because of inaccurate cover metrics for three plots whose photogrammetric point clouds had high vertical bias with respect to the lidar ground model ($r^2 = 0.66$ after vertical bias correction).

Based on the results in Figure 3 and Figure *4*, we expected the indicator of canopy consumption (*AvgCC*) to be a significant factor in models of forest structure attributes of burned stands. However, including *AvgCC* in lidar-based regression models of structure attributes increased the percent of variance explained by less than two percentage points. *AvgCC* or its interactions often had small coefficients and were only significant in the models of maximum tree height, Lorey's height, and basal area (Table 4).

3.2 Comparison of lidar and photogrammetric point clouds for unburned plots

Comparing height distributions and metrics derived from the lidar and photogrammetric point clouds of unburned plots revealed trends consistent with their respective methods for sampling the forest canopy (Figure 5). Percentile height metrics (*p25*, *p50*, *p75*, *p90*, *Hmax*) that are relatively closer

to the top of the canopy had slopes closer to one and had higher correlations. Maximum height (*Hmax*, i.e. 100th percentile) had a strong positive relationship with many points falling near the one-to-one line. The differences in $Hmax_{lidar}$ and $Hmax_{photo}$ were more pronounced for short stands as a result of photogrammetry's tendency to underestimate height in stands where HMAX was less than 10 m (Figure 3). In one plot, noise from false image matching led to *Hmax* being much higher for photogrammetry. However, in reviewing the photogrammetric point cloud we found noise from poor image matching more commonly resulted in points below the ground level than above the actual tree canopy. Since these noise points were below the 2m cutoff they had no effect on height metrics unless there was also a high positive vertical bias. Height histograms of individual plots (not shown) revealed that photogrammetry-based point clouds tended to be clustered around a single height level with a few points generated much higher or lower in the canopy, which sometimes resulted in long tails in the height distribution. These compact but long-tailed height histograms from photogrammetry also affected height variability metrics. Photogrammetry derived point clouds tended to have a lower interquartile range, but a greater skew and kurtosis than lidar. Density metrics from lidar and photogrammetry had fairly high correlations of 0.63 to 0.9 despite photogrammetry-based metrics being saturated near 100% for many plots. Photogrammetry-based cover metrics ($cover_{photo}$ and $density_{photo}$) also had a stronger relationship to lidar first returns ($cover_{lidar}$) than to all returns ($density_{lidar}$). As with the height percentile metrics, the density layer metrics, such as *d01* and *d02*, showed slopes closer to one and higher correlations for higher vertical layers.

For unburned plots, lidar and photogrammetry metrics had similar levels of correlation with the field-estimated structure attributes (Figure 6), with lidar having correlations that were greater in magnitude by only 0.11 on average. The absolute maximum correlations between the metrics and the field attributes were also similar across datasets, having a difference of less than 0.1 for all attributes. However, lidar density metrics had higher maximum correlations with every field attribute, and lidar

height variability metrics also had higher absolute maximum correlations with all attributes except canopy base height and basal area. Although maximum correlations were similar between lidar and photogrammetry the identity of the most strongly correlated metric differed in some cases. For example, aboveground biomass was most strongly correlated with $p50_{lidar}$ and $p75_{photo}$. As with the comparison of lidar and photo generated height metrics, the correlation of height metrics with field attributes was higher for height metrics that reflect the distribution of the uppermost canopy (e.g. max height from field data or higher percentile heights from point clouds derived from either source). The difference in the magnitude of correlation between lidar and photogrammetry metrics with field attributes also decreased with increasing height percentile.

3.3 Estimates of forest structure attributes from lidar and photogrammetry

3.3.1 Estimates from lidar

As expected, regression models from post-fire lidar predicted forest structure attributes on unburned plots more accurately than on burned plots, particularly for aboveground biomass, basal area, and canopy bulk density (Table 5). On unburned plots, lidar-based models had fit and prediction accuracies on par with results from Hall et al.'s study (2005) in a similar forest in Colorado. On burned plots, lidar-based models of height attributes had moderately lower prediction accuracy relative to their unburned counterparts, with %RMSE higher by 8.1 percentage points for maximum height, 12.1 for Lorey's height, and 4.1 for canopy base height. With one exception (canopy base height on burned plots), a single height variable was selected for models of height attributes. This made them more robust than the models of aboveground biomass, basal area, and canopy bulk density which relied on both height and density metrics that were affected by canopy consumption. The ability of lidar-based models to predict these other forest structure attributes on burned plots declined more substantially, with an increase in %RMSE of 16.4 for basal area, 15.7 for aboveground biomass, and 22.8 for canopy bulk density. Models of these structure attributes relied on both height and density metrics, which made

them more susceptible to weaker relationships between these metrics and the canopy structure of burned plots. This is a reflection of the effect of crown consumption on lidar density metrics and, to a lesser extent, height metrics which are shown in Figure *4* and Figure 3, respectively.

3.3.2 Estimates from photogrammetry

For unburned plots, the explained variance (Adj R^2) and prediction accuracy (%RMSE) for models predicting structure attributes was nearly equivalent for photogrammetry and lidar-based models for most structure attributes (Table 5). $Hmax_{lidar}$ had nearly a one-to-one relationship with maximum tree height and a measurement bias of 0.8 m and standard error of 1.6 m while $Hmax_{photo}$ had a bias of 0.2 m and a standard error of 2.7 m (Figure 3). With an intercept of 4.95 and a slope of 0.64, the regression line for maximum tree height from photogrammetry would suggest that height was underestimated when trees were shorter and overestimated when trees were taller, but the line was strongly leveraged by a single outlier because of noise from poor image matching. This outlier also had a strong influence on the photogrammetry-based model of Lorey's height which used $Hmax_{photo}$ as the selected variable. As a result, Lorey's height was more accurately predicted with lidar (%RMSE = 12.3) than with photogrammetry (%RMSE = 16.2). Dropping the outlier improved photogrammetry's estimate of maximum tree height (%RMSE = 11.15, slope = 0.7, intercept = 4.3) and Lorey's height (%RMSE = 13.38). Surprisingly, the difference between lidar and photogrammetry on unburned plots was lower for basal area and aboveground biomass (<2.1 percentage point difference in %RMSE) than it was for the height attributes (3.1-5.6 difference in %RMSE).

Since the stereo imagery was collected before the fire, models derived from photogrammetry had similar performance in burned and unburned areas as opposed to the substantial declines in model performance we observed for post-fire lidar in burned areas. Photogrammetry-based models on burned plots had a %RMSE within less than 10 percentage points of unburned plots for all attributes except aboveground biomass and canopy bulk density (Table 5). Even though photogrammetry's prediction

accuracy of aboveground biomass was worse on burned plots (%RMSE=41.9) than unburned plots (%RMSE = 31.0), this method was still more accurate than estimates from the post-fire lidar (%RMSE = 45.0). Although photogrammetry-based models performed better than lidar on burned plots, it's improvement over lidar varied considerably across the structure attributes. On burned plots, the %RMSE of the photogrammetry-based models was lower than lidar by 0.8 percentage points for maximum tree height, 5.6 for Lorey's height, 11.1 for basal area, 3.1 for aboveground biomass, and 3.2 for canopy bulk density.

3.3.3 Estimates of canopy fuels from lidar and photogrammetry

Models of canopy bulk density on unburned plots had only modest prediction accuracy for both lidar (%RMSE = 36.7) and photogrammetry (%RMSE = 36.8), with the *cover* metric being the only independent variable selected for both datasets. Canopy base height was also more accurately predicted by lidar, but both models had an RMSE of less than one meter. Photogrammetry-based models that included texture and vegetation indices during model selection for canopy bulk density also retained *glcm_mean* on unburned plots and *glcm_contrast* on burned plots, but their inclusion did not substantially improve prediction accuracy. Texture and vegetation metrics were dropped from all other models as a result of the best subset selection process. Their results are not shown for other structure attributes since they were identical to the photogrammetry-based models which did not include these metrics in the selection process. We also regressed the residuals from every model on a set of topographic indices and species composition to test for model biases. These additional metrics explained an average 4% of the variance in the model residuals (range = 0 - 24%), and they had no consistent relationships with the attributes across burn severities or data sets.

3.3.4 Estimates from combined photo and lidar dataset

On unburned plots, lidar and photogrammetry-based models appeared to have only minor differences between selected variables and their relationship to the structure attributes. To test if these

differences between datasets were meaningful, linear models were generated using a dataset containing two copies of each unburned plot; one which had lidar metrics and the other with photogrammetry metrics (Figure 7). Using the predicted structure attributes, a second regression analysis examined the effect of the source of the data (photo or lidar) and the interaction of the source and the predicted value to test for significant intercept and slope bias. We evaluated combinations of variables with one from each metric category to determine which combinations explained the greatest variance while having insignificant levels ($p > 0.05$) of intercept bias (i.e. intercept not equal to zero) and slope bias (i.e. slope not equal to one) introduced by the source (Table 6). For basal area, aboveground biomass, canopy bulk density, and canopy base height we found subsets of variables which explained relatively high levels of variance while the data source was insignificant. For these variable combinations lidar and photogrammetry were nearly interchangeable in predicting the forest structure attribute. Data source was significant ($p < 0.05$) for all regressions of maximum height using height metrics and all linear models of Lorey's height except those that explained very little variance. For these attributes we show the model with the maximum r-squared since regressing on data source with these models introduces reasonably low slope and intercept bias even though they are statistically significant.

3.4 Reconstructing forest structure prior to the High Park Fire

We mapped pre-fire forest structure over the High Park fire burn scar and surrounding area using the pre-fire aerial photogrammetry-based models calibrated from the unburned plots (Table 5a). Mapped values were forced to zero when canopy metrics were zero since these areas should not be forested. These maps were used to assess the potential influence of pre-fire forest structure on burn severity and calculate the loss of live aboveground biomass. The maps of forest structure have several small omissions in coverage due to gaps in the lidar-based ground model and unsuccessful matching of some image areas by the photogrammetry software. These gaps total 54.3 hectares and amount to less than 0.3% of each burn severity's area. The photogrammetric point cloud also had an apparent vertical

bias of greater than 2 m above the lidar ground model in several patches within the burn perimeter, which covered a total area of approximately 15 km^2 (~4% of the burn area). The vertical bias in these areas led to overestimation of basal area and canopy bulk density because of inflated values of the canopy cover metrics used in the models for these structure attributes. The variability in vertical bias across the study area prevents us from correcting this difference without incorporating more ground control points during triangulation; 40 control points were collected from lidar intensity and DTM images to triangulate the 15 flightlines.

The map of aboveground biomass (Figure 8) shows pre-fire biomass to be high in drainages, in the dense stands of lodgepole pine in the southwest portion of the burn scar, and on northern aspects of ponderosa pine and Douglas-fir stands in the eastern portion of the burn scar. Given that approximately 17% of the High Park area was impacted by mountain pine beetle in the three years prior to the fire (Stone, 2015), our map actually estimates the live aboveground woody biomass prior to the fire and beetle epidemic. Maps of the beetle epidemic (Stone, 2015) would allow us to calculate loss of live biomass due only to beetle kill if we assumed a fixed level of mortality in each cell (e.g. 100% mortality), but mortality level likely varied between cells. Instead we focus on the biomass lost in the fire by assuming complete mortality in high and moderate burn severity areas and ignore that the biomass estimated for the pre-fire condition may have been alive or dead and standing. Visual inspection of post-fire imagery indicates that there was also some mortality in low burn severity areas. Tree mortality in these areas could have been directly caused by fire damage, or delayed mortality due to insects, disease, drought stress, or other agents as an indirect result of fire damage weakening the tree's defenses. The rate and cause of mortality could be investigated with the multi-temporal hyperspectral imagery collected over the burn scar and additional field surveys, but for this study we assume 0% mortality in low burn severity areas to make a conservative estimate of biomass lost in the fire. Figure 9 shows the percent of the total burn area covered by each burn severity and the percent of total pre-fire

biomass in that burn severity category. We estimated the pre-disturbance live aboveground woody biomass to be 3.26 Tg within the burn perimeter, with 2.16 Tg killed in moderate and high burn severity areas. Assuming that carbon was 50% of biomass, 1.08 Tg of carbon were transferred to other carbon pools such as standing dead biomass, coarse woody debris, and emissions. This amount of carbon is roughly equivalent to the amount produced by a single coal power plant in a year (US EPA, 2014).

Areas that burned at different severity levels had minor differences in most pre-fire forest structure attributes (Figure 10). Since our data represent a census of the structure and burn severity conditions, we refrained from using tests of significance in our analysis and instead focus on effect sizes. Pre-fire aboveground biomass and basal area had slightly higher median values in high burn severity areas (AGB median = 108 Mg ha^{-1}, BA median = 25 m^2 ha^{-1}) than in other burn classes (AGB medians = 71 to 82 Mg ha^{-1}, BA medians = 16 to 18 m^2 ha^{-1}), but a high degree of overlap in interquartile ranges indicates the differences in structure across burn severities were still relatively minor. Canopy bulk density had bimodal distributions for all but high burn severity because the model was based on canopy cover which was often near 0% or 100% since photogrammetry can only sample the ground through large gaps in the canopy. While this meant that estimates of canopy bulk density saturated at 100% canopy cover, our estimates of canopy bulk density across burn severities still indicated that a continuous canopy was necessary to carry a high severity crown fire. This can be seen by the higher median and lack of low canopy bulk density values for the high burn severity category. Canopy base height, Lorey's height, and maximum height had similar medians for all burn severities, but an increase in burn severity corresponded to a smaller interquartile range and a decrease in the frequency of low height values in favor of a more pronounced single peak near the median height. This is another indication that open uneven-aged stands and areas dominated by shrubs, both of which had lower height values, were less likely to carry a high severity crown fire.

Distributions of forest structure across burn severities were also partitioned into areas burned under severe and calm weather conditions (Figure 11). Nightly thermal imaging collected by the National Infrared Operations (NIROPS) team was used to map the daily burn perimeter, which we obtained from the Geospatial Multi-Agency Coordination website ("GeoMAC Wildfire Map," 2012). Wind gust speeds from three nearby Remote Automated Weather Stations (RAWS) were averaged over the time period between NIROPS observations and compared to the corresponding area burned (Figure 12). According to these burn perimeters and weather data, the fire covered 150.8 square kilometers (~42 % of the total area) in the first two days during an intense wind storm, and it progressed more slowly to burn the remaining area over the next 21 days. We partitioned the dataset into areas that burned under these severe weather conditions in the first two days and under calmer weather conditions in the remaining days to examine possible differences in forest structure across burn severities under different weather conditions. However, the distributions show no substantial differences between the weather classes when looking at the forest structure of the burn severity classes (Figure 11).

4 Discussion

4.1 Effect of crown consumption on lidar height and density estimates

Lidar collection of our study area was intended to characterize the burned forest canopy, but consumption of tree crowns by the fire reduced canopy surface area and reflectance which resulted in few canopy returns and slightly lower height measures. Lidar is known to underestimate individual tree heights by about 0.4 to 1.2 meters for the dominant species found in our study area due to laser pulses missing tree tops or insufficient energy being returned until the pulse reaches lower in the canopy (Andersen, Reutebuch, & McGaughey, 2006). Underestimation is partially a function of crown geometry, with narrow leaders from trees like Douglas-fir more likely to be missed by a laser pulse than the broad tops of trees like ponderosa pine (Andersen et al., 2006), but the degree of error also depends on lidar collection parameters such as pulse repetition rate (Chasmer, Hopkinson, Smith, & Treitz, 2006) and beam divergence (Andersen et al., 2006). An increase in either of these collection parameters will reduce the power associated with each pulse. Burned snags have a much lower surface area and reflectance than typical tree crowns making them a difficult target to measure with lidar. A previous lidar collection of our study area in 2012 had inadequate pulse density and laser power for obtaining lidar returns from burned canopies, but various changes to flight parameters, such as a decrease in flight altitude, substantially increased lidar canopy returns for the dataset used in this study.

Our results suggest that with adequate post-fire lidar sampling it is possible to obtain reasonable estimates of height for burned snags, which should also reflect pre-fire canopy height for areas of similar vegetation and disturbance. Based on prior studies, we expected high underestimation of canopy height by the post-fire lidar, but canopy consumption had only a minor effect on lidar height metrics. Wulder et al. (2009) found significant reductions in lidar measured canopy height following fire in boreal forests, which is presumably due to laser pulses having greater penetration into the canopy before a significant amount of energy was returned. Bolton, Coops, and Wulder (2015) examined a chronosequence of burn

patches with discrete return lidar transects spanning Canada's boreal forests, and they observed higher canopy heights in unburned areas than areas that burned within a five year period prior to the lidar collection. The methods of our study were more similar to Wing et al. (2010), who examined the accuracy of measuring burned snags in ponderosa pine forests of the Pacific Northwest with discrete return lidar and reported height accuracies of 2.8-4 m (RMSE). For our study, lidar estimates of maximum height had an RMSE of only 2.6 m in burned plots (Figure 3), which is lower than would be expected given the results of the aforementioned studies. Maximum tree height was noticeably underestimated in only three of the severely burned plots. $Hmax_{lidar}$ was actually higher than the field-measured maximum height in 62 % of the plots across both burn severities, with an average difference of 1.5 m when the point cloud metric was higher than the field measure. The overestimation of height is consistent with edge effects, which may result from GPS error and trees outside the plot having a portion of their canopy overlapping the plot area. Edge effects are more likely to be a significant problem with smaller plot areas (Zolkos, Goetz, & Dubayah, 2013), but high spatial variability in tree heights may cause significant edge effects even with moderate plot sizes such as the 400 m^2 plots used in this study.

The loss of needles and fine branches in high burn severity areas reduced lidar cover below expected pre-fire cover levels for a given field-measured tree density. The fire reduced canopy volume by various amounts on burned plots which we quantified in a relative index as the average of field estimated crown consumption for individual trees (*AvgCC*). This loss of canopy volume was associated with fewer lidar returns from the canopy, which made $cover_{lidar}$ a less reliable predictor of pre-fire tree density. While only $cover_{lidar}$ and tree density are shown as examples, other lidar density metrics appeared to be affected by canopy consumption as well, which likely reduced the explanatory power of these metrics in estimating pre-fire forest structure attributes. Wulder et al. (2009) also observed significant declines in lidar measures of canopy cover following wildfire and found this change to be

strongly correlated with burn severity as measured by the differenced normalized burn ratio (dNBR) index. When examining a chronosequence of burned patches with discrete return lidar transects, Bolton et al. (2015) found canopy cover to be much higher in unburned areas than areas that burned within the last five years. Similar results have been found in studies of deciduous forests where lidar collected during leaf-off conditions underestimated leaf-on fractional cover (Wasser, Day, Chasmer, & Taylor, 2013), as one would expect.

The results from this analysis led us to model unburned and burned areas separately when estimating forest structure attributes as described in section 3.4. Although we chose a threshold of 50% in average crown consumption for assessing the influence of burn severity on lidar metrics, it is more likely that canopy consumption influenced lidar metrics on a continuum. Pre-fire RapidEye imagery failed to produce accurate estimates of pre-fire canopy cover which would be necessary to map canopy consumption for the study area. Instead of relying on image-based estimates of change in canopy cover, we decided to model structure attributes separately for burned areas and unburned areas.

Incorporating information on canopy consumption failed to improve lidar-based models of forest structure despite its apparent influence in the prior analysis. The effect of canopy consumption on lidar, which we observed in Figure *4* suggested that we could test for the significance of this factor by including it as an independent variable or interaction in regression models. *AvgCC* was statistically significant in some models, but its inclusion had very little effect on model fit. *AvgCC* may have had little explanatory power because it was a relative index based on visual estimates of consumed vegetation from tree crowns. Although *AvgCC* served as an adequate index for identifying severely burned plots, it did not complement the post-fire lidar density metrics well enough to explain additional variance in forest structure. An absolute measure of the proportion of canopy cover consumed by the fire may have proven more informative and significant in the regression models, but it would not be possible to calculate this without pre-fire field or lidar measurements.

4.2 Comparison of lidar and photogrammetry metrics

On unburned plots, photogrammetry-based height metrics were strongly correlated with those from lidar, while height variability metrics exhibited weaker correlations between datasets due to photogrammetry's dense sampling of points on the canopy surface. Image matching can only occur for objects observed from multiple camera positions which restricted point generation to locations on the canopy surface and where large gaps occur in the canopy. Due to this restriction, points become concentrated in a single layer draped over the canopy with few points representing objects that may be present under the canopy surface. We found that the photo point cloud led to a height distribution with a lower standard deviation, higher kurtosis, lower maximum height, and higher values for height percentiles when compared to lidar.

Photogrammetry generally yielded density metrics with much higher values than lidar, as found in other studies. Lidar is known to yield canopy cover estimates which correspond closely with field measurements (Korhonen et al., 2011), but photogrammetry can greatly overestimate cover. The spatial arrangement of crowns and the percent of overlap between subsequent camera frames affects photogrammetry's ability to sample the ground topography and accurately represent canopy cover. For example, photogrammetry would likely produce more accurate cover estimates on a plot with 50% cover if the canopies were clustered together with a single large gap, than if the canopies were evenly spaced with small gaps between them. Increasing the image overlap reduces the ground area occluded by tree canopies in multiple images and may improve image matching because of greater similarity between adjacent frames. This should enable photogrammetry to yield more accurate estimates of canopy cover, but this has yet to be tested. Increasing image overlap also decreases the base-to-height ratio of image collection which is expected to reduce the accuracy of height measurements, but previous studies have found only minor differences in height accuracy when comparing different overlap percentages (Bohlin et al., 2012; Nurminen et al., 2013). Because of the 60% forward overlap used for

our study, photogrammetry sampled the ground only through large canopy gaps which resulted in much higher values of overall canopy density, such as $cover_{photo}$ and $density_{photo}$, and density metrics in the height range of most dominant trees (*d02* for most of our plots). This also led to much lower values of density for low canopy layers (e.g., *d01*) and a weaker correlation with the values observed by lidar at those levels. Vastaranta et al. (2013) also found a decrease in the difference between lidar and photogrammetry cover metrics with increasing canopy height interval, but they did not directly compare metrics for individual plots as we have in this study.

Errors in point cloud generation were another important determinant of the observed differences in lidar and photo point cloud metrics for some of our plots. Despite a low overall RMSE (1.09 m) from triangulation checkpoints and a reported vertical error of 0.82 m, the point cloud for some plots still had a vertical misregistration to the lidar of up to 2.5 m. The high variation in terrain for our study area (50% of the burn area has slopes greater than 20 degrees) makes some vertical bias likely, and this should be considered before applying this observation to sites with lower slope. A high positive vertical misregistration can cause points on low vegetation and ground to be pushed above the 2 m height cutoff. In areas of low canopy cover this may result in an anomalously high number of observations near the terrain surface which 1) decreases height metrics, 2) increases height variability metrics, and 3) increases the general and low layer density metrics (*density/cover* and *d00*). We attempted to manually apply a vertical correction to the photogrammetric point cloud on 17 plots by visually matching the apparent photogrammetric ground points to the lidar ground points. This correction caused only minor increases in correlation and slope for most metrics, so we continued our analysis without the correction.

In contrast to the minor differences caused by vertical registration errors, failure of the image matching software to generate points on the canopy surface had a much stronger impact on the height distribution of points and their derived metrics. In 31 unburned plots we observed areas of the point

cloud where canopy points appeared to be either missing or at a much lower height than the canopy surface detected by lidar. Gruen (2012) lists a number of potential issues that can lead to poor image matching results including poor image texture such as in shadows, a lack of planar facets on objects, and repetitive objects, which are all common features of tree canopies in imagery. We observed poor image matching results most often on plots with relatively short and isolated trees. This effect can be seen in height metrics such *Hmax*, which had low values from photogrammetry on plots where the lidar *Hmax* was less than 10m (Figure 5). Adjacent camera frames may have observed different sides of an isolated conifer rather than a continuous canopy surface, and the dissimilarity in pixel patterns from different camera angles could have prevented successful point generation for these trees. It is also possible that potential points on isolated trees were automatically filtered out by the image matching software as noise. Poor image matching results for a plot likely decreased height percentiles and could have either increased or decreased various density and height variability metrics with regard to expected values from perfect image matching results. Plots in which the height metrics from photogrammetry were lower than from lidar appeared to have poor image matching results, vertical misregistration, or both.

Improvements in image matching are leading to more accurate and complete photogrammetric point clouds (Gruen, 2012), but the problems we observed are unlikely to be resolved in the near future given the numerous challenges associated with image matching for forested scenes. Current image matching techniques perform well for images of developed landscapes, where objects are spatially distinct and have well defined edges. Trees in forested landscapes may have overlapping crowns and repeated patterns (e.g. in areas of similarly sized trees) that lead to fewer matches between images and erroneous matches. In open forests, the spatial mosaic of sunlit and shadowed crowns and background cover further complicates image matching, especially when two stereo images view opposite sides of a partially sunlit tree. Incorporating this information into matching algorithms could lead to an improvement in point cloud and DSM accuracy over forested areas, particularly in sparse stands. These

problems may make photogrammetry less reliable than lidar under some circumstances and should be considered alongside other factors when evaluating technologies for mapping forest structure over broad extents.

We expected the strength of the relationship between a forest structure attribute and photogrammetry-based metrics to depend on the attribute's association with the canopy interior and the success of image matching. As in prior studies (Gobakken et al., 2015; Järnstedt et al., 2012; Pitt et al., 2014; Vastaranta et al., 2013), we found stronger relationships between height attributes (HMAX, HLOR, and CBH) and lidar-based metrics than photogrammetry-based metrics (Figure 6). The advantage of lidar could be due to a more accurate sampling of the canopy surface or its ability to sample the full canopy profile. Some height attributes may be more strongly associated with height metrics representing the distribution of the full canopy profile, which is better captured by lidar, rather than metrics that only represent the distribution of the canopy surface, which can be adequately measured with photogrammetry. Since canopy bulk density is based on the mass of materials in the canopy profile we expected lidar metrics to have higher explanatory power than photogrammetry for this attribute, but all the photogrammetry height metrics and three of the variability and density metrics (*iqr*, *density*, and *d02*) had higher correlations with canopy bulk density by 0.06 to 0.13. Lidar *cover* was the notable exception which had the highest absolute correlation (r=0.67). This could indicate that sampling of the canopy interior provides little or no benefit for estimating canopy bulk density and that canopy cover metrics may be the best predictor of canopy bulk density in similar forests. However, in plots with low tree density photogrammetry may sample points on the sides of tree crowns causing height and height variability metrics to be influenced by crown length in such a way that these metrics become more strongly associated with canopy bulk density. Lidar density metrics also had higher correlations with other attributes such as basal area and aboveground biomass, which are often related to canopy cover. Density metrics from photogrammetry may saturate at relatively low canopy cover much in the same

way that NDVI saturates at moderate levels of leaf area index (Carlson & Ripley, 1997). Even with this cover saturation effect, we expect photogrammetry to more accurately predict structure attributes in forests of continuous canopy cover and our results support this.

4.3 Estimation of forest structure attributes

4.3.1 Comparison of photogrammetry and lidar for estimating forest structure of unburned areas

Models of forest structure derived from lidar metrics on unburned plots had accuracies consistent with literature values for most attributes and therefore can serve as a standard basis for comparison to other model scenarios. Although our lidar estimates of aboveground biomass did not meet the suggested accuracy level of less than 20 Mg/ha or less than 20% RMSE for carbon monitoring (Goetz & Dubayah, 2011), they are similar to many previous studies which also fail to meet this standard (Zolkos et al., 2013). This standard remains a challenging goal for using remote sensing to aid carbon accounting efforts. Since most other attributes also had accuracy levels on par with previous studies in similar forests, models from lidar on unburned plots serve as our basis for comparison with photogrammetry and with lidar on burned plots.

Photogrammetry-based models performed similarly to lidar on unburned plots for all forest structure attributes. The lidar-based model of aboveground biomass had higher prediction accuracy than photogrammetry, but the difference between them was lower in our study than the differences reported by St-Onge et al. (2008) and Vastaranta et al. (2013) (1.7 percentage points difference in %RMSE vs 4.2 and 6.2 percentage points, respectively). As with prior studies (Gobakken et al., 2015; Järnstedt et al., 2012; Nurminen et al., 2013; Pitt et al., 2014; Vastaranta et al., 2013), lidar-based models also had slightly higher accuracy than photogrammetry-based models for some other attributes such as Lorey's height, but photogrammetry had slightly higher accuracy than lidar for estimating basal area in this study. Most lidar – photogrammetry comparisons to date have taken place in boreal forests which may possess more continuous canopies than the savannah-like southern aspects of our study

area. A more continuous canopy surface could reduce the potential for errors in the photogrammetric point cloud, which we observed mainly on plots with low tree density. However, the Norway spruce (*Picea abies*) of boreal forests may feature more narrowly conical crowns than the dominant species in our study area, ponderosa pine. Trees with narrow peaks may suffer from greater underestimation of canopy height than broadly peaked trees because of failure to match pixels on small terminal leaders. The effect of crown shape and collection parameters on tree height estimation has been studied extensively for lidar (Andersen et al., 2006), but to our knowledge, no studies have evaluated individual tree height accuracy from photogrammetry for different collection and processing scenarios. A thorough comparison of tree and stand height accuracy from photogrammetry under different forest types and conditions, collection parameters, and image processing methods would greatly aid operational use of photogrammetry in forestry as it has with lidar.

Photogrammetry may also be useful for predicting canopy fuels which are commonly thought to be associated with canopy interior measures that can only be provided by lidar. Photogrammetry-based models predicted canopy bulk density with nearly the same accuracy as lidar in unburned areas, and lidar sampling of the canopy interior appeared to provide no benefit since percent cover of first returns (*cover)* was the only lidar metric selected. However, the lidar-based models of canopy bulk density on unburned plots had a surprisingly low R^2 of 0.44 compared to some prior studies which had R^2 values between 0.67 and 0.84 (Andersen et al., 2005; Erdody & Moskal, 2010; Hall et al., 2005; Hermosilla et al., 2014), but our %RMSE of 36.7 was lower than the 38% reported by Hermosilla et al. (2014). Canopy fuel attributes are defined and calculated differently across studies which adds to the uncertainty in making comparisons between them. To our knowledge, our study is the first to estimate canopy fuels with a photogrammetric point cloud, and we were surprised to find predictive accuracy similar to lidar. Fuel maps are frequently used in fire behavior modeling but recent lidar coverage is rarely available and expensive to collect, while aerial photography is widely available and collected frequently. If canopy

fuels can be reliably estimated from lidar because of their relationship to canopy height and cover then photogrammetric point clouds may hold the same capability. The Landscape Fire and Resource Management Planning Tools program (LANDFIRE) provides maps of canopy fuels for the United States which are derived from Landsat data and biophysical gradient modeling, but these maps are better suited for regional to national level planning rather than for landscape scale usage (Reeves, Ryan, Rollins, & Thompson, 2009). The higher resolution and accuracy provided by lidar or photogrammetry could greatly aid land managers in reducing the risk of catastrophic fires and understanding the spatial relationship between pre-fire canopy fuel distribution and burn patterns. If there are consistent relationships between canopy fuel indices and metrics derived from photogrammetric point clouds, they could serve as training datasets for future national level mapping efforts.

The similarities between lidar and photogrammetry discussed above could make them interchangeable for many purposes. Although we observed differences in point cloud metrics for lidar and photogrammetry as discussed in section 5.2, for some metrics these differences were small in comparison to their relationship with forest structure attributes. In models combining the lidar and photogrammetry datasets on unburned plots, some combinations of metrics had a similar enough relationship to the structure attributes that data source was not statistically significant (Table 6, Figure 7). The relatively small intercept and slope bias introduced by the source variable in these models was another indicator that data source did not play a substantial role in defining the relationship between some combinations of point cloud metrics and the structure attributes. Furthermore, in this study we looked for consistent relationships between lidar and photo derived metrics so we could evaluate the use of current datasets to interpret historical photos, but in most applications there would be no need for consistency. A consistent relationship between lidar and photo derived metrics should enable us to apply existing lidar models to historical photos for estimating past forest structure, but of all possible metric combinations we found very few to be directly interchangeable between the lidar and

photogrammetry datasets in modelling forest structure. For this application to be reliable, the linear relationships we observed in comparing lidar and photo metrics would need to be consistent across datasets with different collection parameters. Calibrating models from modern imagery with similar scale and overlap to a historic photo collection may be a more reliable approach to estimating historic forest structure.

The similarity between the prediction accuracy for lidar and photogrammetry for unburned areas in this study lends weight to the growing evidence that a combination of a lidar ground model and photogrammetric point cloud could serve as a suitable alternative to repeated lidar surveys for updating forest inventories. The difference in predication accuracy between lidar and photogrammetry in unburned areas was negligible for aboveground biomass, basal area, and canopy bulk density, although height attributes were predicted with slightly higher accuracy by lidar (e.g. 16.2% vs 12.3% RMSE for Lorey's height in unburned plots, Table 5). This relatively small difference in accuracy and the lower collection cost should make photogrammetry an appealing alternative to lidar for updating forest inventories where an accurate digital terrain model is available. This application has already been tested and emphasized in several studies (Bohlin et al., 2012; Gobakken et al., 2015; Järnstedt et al., 2012; Nurminen et al., 2013; Vastaranta et al., 2013). Although lidar coverage is still rare, digital terrain models from nationwide lidar collection programs, such as the 3D Elevation Program (3DEP) in the United States, could enable the use of photogrammetry for future updating of forest inventories across broad spatial extents to aid forest management and estimate carbon sequestration. Numerous aerial and stereo satellite image collections are already available to support this application. For example, the National Agriculture Image Program (NAIP) annually collects aerial imagery over large portions of the United States at a one meter ground sampling distance, which may be sufficient to map forest structure attributes with similar accuracies to those obtained with the 30 cm resolution imagery used in this study.

At a global scale, a single global DTM collection, as would be provided by the Lidar Surface Topography mission (Yu et al., 2010), would enable flexible approaches to mapping canopy height and biomass using a variety of stereo data sources to map canopy elevation. DTMs derived from radar interferometry, such as the Shuttle Radar Topography Mission product (Farr et al., 2007) or WorldDEM-DTM ™ product developed from the TanDEM-X mission (Riegler, Hennig, & Weber, 2015), are unsuitable because they do not penetrate to the terrain surface in forested areas. These limitations also apply to interferometry using longer wavelengths, which do penetrate the canopy, since volume scattering is likely to reduce coherence between the return signals (Rodriguez & Martin, 1992). Similarly, DTMs generated from ALOS PRISM such as the AW3D™ product (Tadono et al., 2014) or higher resolution imagery are also unsuitable as they sample only the uppermost canopy surface. On the other hand, these same sensors, as well as many other high spatial resolution airborne and spaceborne sensors, are likely to be suitable for mapping the elevation of the canopy surface. With a suitable global DTM, this would allow for the creation of canopy height and biomass estimates at a variety of spatial resolutions and levels of vertical precision. Wall-to-wall products might be produced at a regional scale using canopy elevation estimates from a relatively coarse imager such as JAXA PRISM, while higher precision products could be produced on a local or project scale using airborne or higher resolution satellite stereo imagery. Such an approach would likely be more cost-effective than repeated surveys with lidar remote sensing.

Others have suggested the application of combining previously collected lidar data with future image collections as discussed in the previous paragraph, but the potential to apply this method to past image collections for historical analysis of forest change has been largely overlooked. To the knowledge of the authors, Vega and St-Onge (2008) are the only researchers to have successfully demonstrated application of combining photogrammetry with lidar in a historical context by measuring changes in canopy height with a series of aerial photos from 1945 to 2003. Aerial imagery collected for resource

management, such as the imagery used in this study, is widely available in the United States, and the NAIP program began collecting high resolution imagery in 2003. Historic aerial photographs such as the early collections contracted by the Soil Conservation Service, may also be useful if collected at a large-scale and adequately preserved. Applying modern photogrammetry to this large archive of aerial imagery could open the possibility for continental-scale change detection of forest structure starting from the late 1930s. The primary challenge with this approach will be obtaining accurate point clouds from scanned photographs which may suffer from noise, distortions from improper scanning, and degradation from being inadequately preserved.

4.3.2 Utility of vegetation and texture indices in photogrammetry-based models

Including vegetation and texture metrics with photogrammetry-based point cloud metrics failed to improve estimation accuracy of most forest structure attributes. Our variable selection strategy removed vegetation and texture metrics from all but three models, which suggests that these metrics did not explain additional variation in the structure attributes over what could be explained with height and density based metrics from the point cloud. However, our variable selection strategy of grouping metrics and applying correlation-based filtering may have excluded potentially useful metrics. The vegetation and texture metrics had lower within group correlation than the point cloud metrics, and some of these variables may have been selected if metrics were grouped empirically using a technique such as hierarchical cluster analysis. Also, we only produced a small subset of potential metrics that could be derived from the two-dimensional spectral information. A wide variety of spectral indices and different parameterizations of texture indices have proven useful in estimation of forest structure (Tuominen & Pekkarinen, 2005). A thorough examination of spectral and texture indices in this context could be helpful for determining which ones best complement point cloud metrics for modelling forest structure. The high spatial resolution and point density available with aerial imagery also lends itself to object-oriented analysis, which could be used either to provide additional plot level indices or to enable

analysis on the level of individual trees. Simultaneous development of dense image matching algorithms and individual tree delineation techniques presents an exciting opportunity for fully utilizing high resolution stereo imagery.

4.3.3 Comparison of pre-fire imagery and post-fire lidar for estimating forest structure of burned areas

The substantially higher accuracy of photogrammetry-based models on burned plots suggests that this approach may be preferable to post-fire lidar for estimation of pre-fire structure attributes. Lidar-based models of maximum height, Lorey's height, and canopy base height had only modest drops in performance when compared to their unburned counterparts, but models of aboveground biomass, basal area, and canopy bulk density performed much worse on burned plots than unburned plots. The dependency of aboveground biomass, basal area, and canopy bulk density on both height and density metrics likely made models of these attributes more susceptible to declines in performance because of the effect of canopy consumption on both types of metrics. In contrast, estimates of field measured height attributes only depended upon point cloud height metrics and were likely less susceptible to the effects of canopy consumption. These results are substantiated by Figure 3 and Figure *4*, which show density metrics to be more strongly affected by canopy consumption than height metrics. It is unlikely that model performance would improve substantially for these attributes even with higher pulse density or laser power since pre-fire canopy cover information cannot be recovered after the fire from this data.

We expected this decline in lidar-based model accuracy on burned plots because of reports by others of lower canopy height and cover measured by lidar in burned areas (Bolton et al., 2015; Wing et al., 2010; Wulder et al., 2009), but our results conflict with lidar studies of forest structure in leaf-off deciduous forests, which we expected to be similar to burned coniferous forests. Naesset (2005) estimated Lorey's height, basal area, and timber volume in a mixed-forest of Norway with similar accuracies between leaf-off and leaf-on lidar collections. In a study of tropical dry forests, prediction accuracy of aboveground biomass was slightly worse with leaf-off lidar (RMSE = 25.7 Mg ha^{-1}) than with

leaf-on lidar (RMSE = 21.6 Mg ha^{-1}), but the difference in the mean predicted field biomass was insignificant in both cases (Hernández-Stefanoni et al., 2015). Similarly, Anderson and Bolstad (2013) found only minor differences in prediction accuracy between leaf-off and leaf-on lidar when estimating aboveground biomass in temperate deciduous and mixed forests of Wisconsin. The discrepancy between these studies in deciduous forests with leaf-off conditions and our study of burned snags may be due to the branching structure of leaf-off deciduous trees which could still be capable of returning a significant amount of laser energy. Many of the burned coniferous snags likely have lower surface area and reflectance than leaf-off deciduous trees, which led to very few canopy returns in the most severely burned plots.

It may be possible to improve model performance by pairing the post-fire lidar height metrics with pre-fire spectral indices from widely available satellite imagery. However, our tests of incorporating texture and spectral indices with photogrammetry point cloud metrics failed to improve model performance. Combining lidar with optical imagery has improved estimates of aboveground biomass in some studies, but the gains in accuracy are sometimes marginal over using lidar alone (Zolkos et al., 2013).

4.4 Forest structure and the High Park fire

Combining pre-fire aerial imagery with a post-fire lidar ground model enabled us to map aboveground biomass and other forest structure attributes over the High Park burn scar. Maps of other structure attributes (not shown) exhibited spatial patterns similar to that observed on the map of aboveground biomass (Figure 8). Tree height, basal area, and biomass were often highest in drainages. A few of these drainages were spared from burning, possibly because of higher moisture levels or topographic effects on fire behavior, but many patches of high biomass burned at high severity. High burn severity accounted for 43.6% of the total area and 51.3% of the total biomass (Figure 9).

The immediate greenhouse gas emissions from consumption of tree canopies in the moderate and high burn severity areas likely represent a modest fraction of the total emissions from combustion in comparison to the emissions from burning of other carbon pools such as coarse woody debris, understory vegetation, and litter, which were not measured in this study. For example, a study of the 2002 Biscuit Fire estimated live foliage, wood, and bark (including saplings and understory vegetation) to account for only 0.92 Tg of the total 3.83 Tg of carbon emissions (Campbell, Donato, Azuma, & Law, 2007). Through eventual decomposition and subsequent fires, standing dead biomass and coarse woody debris will likely become the largest source of atmospheric carbon resulting from the High Park fire. Global emissions from wildfire were estimated to average 2 Pg of carbon per year between 1997 and 2009 (van der Werf et al., 2010), but may increase with changes in climate. An increase in wildfire activity in the western United States after the mid-1980's has corresponded with early snowmelt and an increase in temperatures which contribute to drought conditions (Westerling, Hidalgo, Cayan, & Swetnam, 2006). These climatic conditions could become more prevalent in the future, increasing global emissions attributable to wildfires and creating a positive feedback loop for climate change (Flannigan, Krawchuk, de Groot, Wotton, & Gowman, 2009). Better accounting of live woody aboveground biomass and other carbon pools could improve estimates of greenhouse gas emissions resulting from wildfires and improve our understanding of fire in the global carbon cycle.

Weather, topography, and fuels drive fire behavior and effects, but the complex interaction of these factors can make it challenging to determine their relative influence on burn severity in individual fires. Schoennagel, Veblen, and Romme (2004) generalized Rocky Mountain forests into three major types of fire regimes (low, mixed, and high severity) and characterized the potential impacts of fire suppression on each of these regimes. Fire suppression is known to have had a significant impact on low elevation dry ponderosa pine forests that have historically burned at low severity but little or no impact on high elevation subalpine forests that historically burned at high severity. There is greater uncertainty

in the effects of fire suppression on mid-elevation mixed conifer forests which have historically burned in complex mosaics of mixed severity (Schoennagel et al., 2004). The High Park burn scar predominately covers forest stands that would be categorized into this mixed severity fire regime. An investigation of fire suppression's role in altering the fuel loads and fire regimes in the High Park area is beyond the scope of this study, but we have examined whether pre-fire forest structure influenced burn severity by comparing the distribution of structure attributes across burn severity classes and under different weather conditions.

We mostly found minor differences in forest structure between areas of different burn severities. However, high burn severity areas predominately had high levels of canopy bulk density as opposed to other burn severity classes which featured both high and low values of canopy bulk density (Figure 10). Since the model of canopy bulk density was solely dependent on photogrammetry-based canopy cover, the high levels of canopy bulk density in high burn severity areas suggests that a continuous canopy was necessary to sustain an active crown fire. Basal area and aboveground biomass tended to be slightly higher in high burn severity areas (Figure 10), which could indicate that areas with high biomass or basal area were more likely to burn at high severity. Much of the high burn severity and high biomass areas were in lodgepole pine stands in the southwestern portion of the burn scar, which typically burn as stand replacing crown fires. Ponderosa pine stands and Douglas-fir stands also burned at high severity as the fire rapidly expanded eastward in the first two days of the fire.

Almost half of the area burned occurred in the first two days of the fire, likely because of an intense windstorm (Coen & Schroeder, 2015). Fuels could have played a more significant role in determining burn severity when weather conditions were not the primary driver of the fire, as was the case in the 2002 Hayman fire in Colorado (Schoennagel et al., 2004). To test this hypothesis we partitioned the burn area into areas burned in the first two days under strong winds and in the remaining days under weaker winds. Excluding large unburned areas inside the burn perimeter, the fire

burned similar proportions of area in each burn severity under strong (Unburned = 13.1%, Low = 16.0%, Moderate = 24.1%, High = 46.8%) and weak winds (Unburned = 12.0%, Low = 16.8%, Moderate = 27.7%, High = 43.5%). The forest structure in each burn severity was also similar for both weather conditions (Figure 11). This indicates that the fire did not preferentially burn areas of high biomass or canopy bulk density when winds were weaker, contrary to our hypothesis. We used daily burn area as a proxy for daily weather conditions, but weather conditions may have influenced burn severity on finer spatial and temporal scales. Understanding the role of fuels, weather, and topography in determining burn severity of the High Park fire may be better accomplished with fire behavior modeling tools or statistical models which include multiple factors. While evaluating all the potential factors which influenced burn severity in the High Park fire was not the intent of this study, our work illustrates the potential for combining photogrammetry and lidar to map pre-fire forest structure which may serve an important role in determining the burn severity patterns of some fires. The ability to retrieve past forest structure has many potential applications which includes enabling land managers and scientists to model fire behavior and effects.

5 Conclusion

Lidar and photogrammetry both served as excellent tools for retrieving forest structure on unburned plots, and post-fire lidar was still capable of recovering canopy height from the remaining snags in burned areas. However, canopy consumption from wildfire reduced the explanatory power of height and density metrics in post-fire lidar which resulted in decreased model performance for structure attributes that depended upon these metrics. As would be expected, photogrammetry-based models from pre-fire imagery performed similarly in plots that were subsequently either burned or unburned, and results from these models were on par with lidar-based models for most structure attributes. These results demonstrate that both post-fire lidar and combining pre-fire photogrammetry with a lidar ground model have the ability to map pre-fire structure in Rocky Mountain mixed-conifer forests. These maps could aid assessment of the spatial relationship between canopy fuels and burn severity and also enable mapping of post-fire effects such as loss of live biomass. Given the low cost and wide availability of aerial imagery, we recommend pursuing photogrammetry as a compliment to lidar for a broader range of applications which require mapping past and present forest structure in similar forest types. With the increasing popularity of high resolution imagery from unmanned aerial vehicles and the growing national lidar collection in the United States, this approach could soon be broadly applied for a much lower cost than repeated lidar collections.

6 Tables and Figures

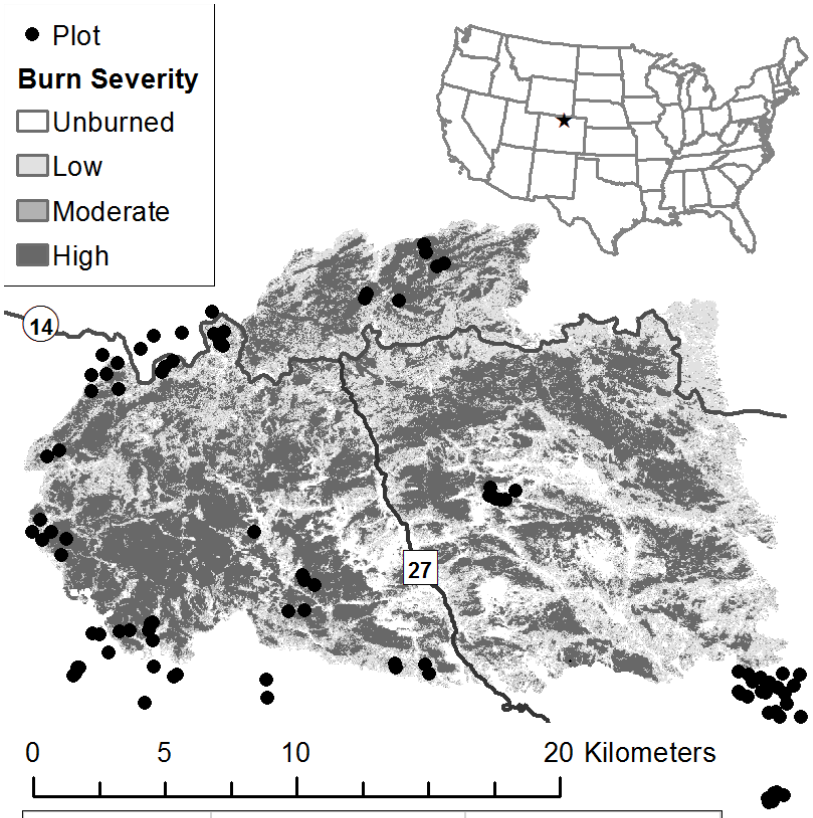

	West	East
Elevation (m)	1900-3100	1600-2500
Burn severity	High	Mixed
MPB severity	High	Low
Ownership	Public	Private
Composition	Lodgepole pine and mixed conifer	Ponderosa pine and mixed conifer

Figure 1. The High Park fire comprised a 35300 hectare area in northern Colorado which was characteristically different across several factors in its eastern and western portions as divided by Country Road 27. Plots were distributed randomly in clusters in areas of different burn severity including unburned areas within and immediately outside the burn perimeter.

Table 1. Summary of field data for structure attributes of interest. Maximum height was not measured on all plots and canopy bulk density and canopy base height were computed only for plots that had PIPO, PICO, or PSME as the dominant species.

	Unburned					Burned				
	Count	**Mean**	**SD**	**Min**	**Max**	**Count**	**Mean**	**SD**	**Min**	**Max**
Aboveground Biomass (Mg ha^{-1})	50	122.8	61.4	2.6	240.0	45	82.5	49.2	12.3	208.4
Basal Area (m^2 ha^{-1})	50	27.5	12.7	0.7	50.9	45	18.0	10.2	3.4	44.4
Canopy Base Height (m)	47	5.5	1.3	2.3	9.3	39	4.6	1.3	2.1	7.2
Canopy Bulk Density (kg m^{-3})	47	0.22	0.11	0.02	0.46	39	0.15	0.12	0.03	0.50
Lorey's Height (m)	50	11.4	3.1	4.4	20.6	45	11.0	3.5	6.3	27.9
Maximum Height (m)	48	14.2	4.2	4.4	21.8	38	13.9	4.7	7.5	32.0
Percent PICO Basal Area	50	23	41	0	100	45	7	24	0	100
Percent PIPO Basal Area	50	49	40	0	100	45	61	35	0	100
Percent PSME Basal Area	50	23	32	0	97	45	23	28	0	96

Table 2. Collection parameters for 2013 lidar and 2008 aerial imagery. Swath pulse density was calculated as the mean density of last returns from individual swaths.

Collection Parameter	**Lidar**	**Imagery**
Sensor	Optech ALTM Gemini	Z/I DMC-1
Flight Altitude above ground level (m)	1000	3200
Number of flight lines	97	17
Side overlap (%)	30	30
Forward overlap (%)	-	60
Scan frequency (Hz)	41	-
Scan angle (degrees)	18.5	-
Pulse repetition frequency (kHz)	70	-
Beam divergence (mrad)	0.8	-
Max returns per pulse	4	-
Swath pulse density (m^{-2})	1.87	-
Number of bands	-	4
Ground sampling distance (cm)	-	30

Table 3. Acronyms for structure attributes and point and image metrics. All point cloud metrics refer to points above the 2m height cutoff. Vegetation and Texture indices apply to the aerial imagery only.

Metric	Description
Structure attributes	
HMAX	Maximum tree height (m)
HLOR	Lorey's height (m)
AGB	Aboveground biomass (Mg ha^{-1})
BA	Basal area (m^2 ha^{-1})
CBD	Canopy Bulk Density (kg m^{-3})
CBH	Canopy Base Height (m)
AvgCC	Average of crown consumed (%)
Point cloud metrics	
Height profile (m)	
Hmin	Minimum height
Hmax	Maximum height
Havg	Mean height
Hqavg	Quadratic average of height
p05, p10, p25, p50, p75, p90	Height percentiles
Height Variation	
stdev	Standard deviation of height (m)
cv	Coefficient of variation of height
skew	Skew of height
kurt	Kurtosis of height
range	Range of height (m)
iqr	Interquartile range of height (m)
Density (%)	
density	Percent of points above the height cutoff
cover	Percent of first returns above the height cutoff
d00, d01, d02, d03, d04	Percent of points within height intervals.
Image metrics	
Vegetation Indices	
ndvi_min	Minimum of NDVI
ndvi_max	Maximum of NDVI
ndvi_rng	Range of NDVI
ndvi_std	Standard deviation of NDVI
ndvi_avg	Mean of NDVI
ndvi_sum	Sum of NDVI
Texture *(based on grey-level co-occurrence matrix (GLCM))*	
glcm_mean	Mean of GLCM
glcm_var	Variance of GLCM
glcm_hom	Homogeneity of GLCM
glcm_contrast	Contrast of GLCM
glcm_dis	Dissimilarity of GLCM
glcm_ent	Entropy of GLCM
glcm_sec	Second Moment of GLCM
glcm_cor	Correlation of GLCM

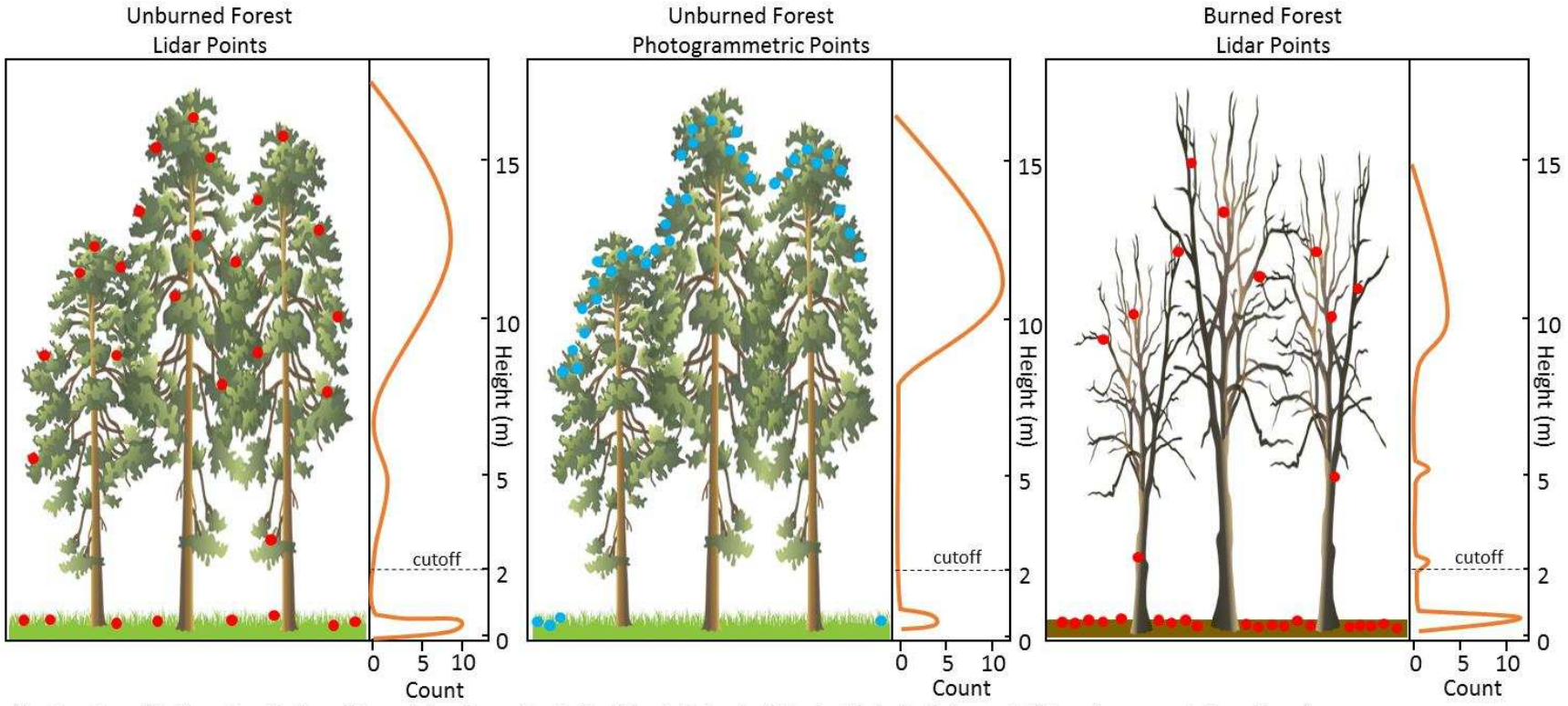

Clipart courtesy of Kim Kraeer,Lucy Van Essen-Fishman, Integration and Application Network, University of Maryland Center for Environmental Science (ian.umces.edu/imagelibrary/)

Figure 2. Hypothetical profiles of point clouds and resulting point height histograms for the three dataset scenarios: lidar in unburned forests, photogrammetry in unburned forests, and lidar in burned forests.

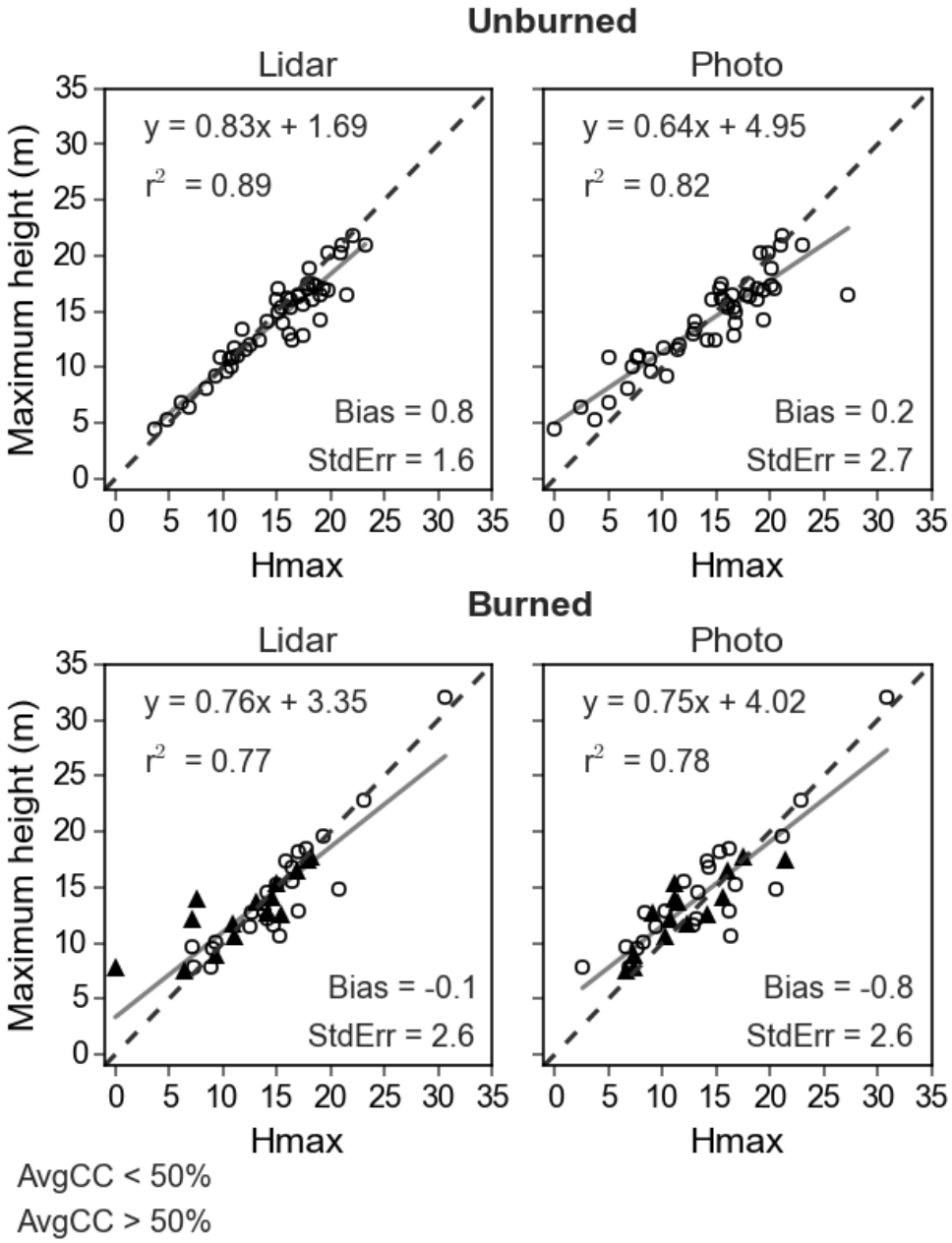

Figure 3. Scatterplots of point cloud maximum height (Hmax) with field maximum tree height (HMAX) for lidar and photogrammetry on unburned and burned plots with the line of best fit (gray) and the 1:1 line (black dashed). StdErr and Bias are with respect to the 1:1 line. Plots with greater than 50% average canopy consumption (black triangle) have similar residuals to plots with less than 50% average canopy consumption (black circle) for both lidar and photogrammetry. All regressions were significant at the 0.05 level.

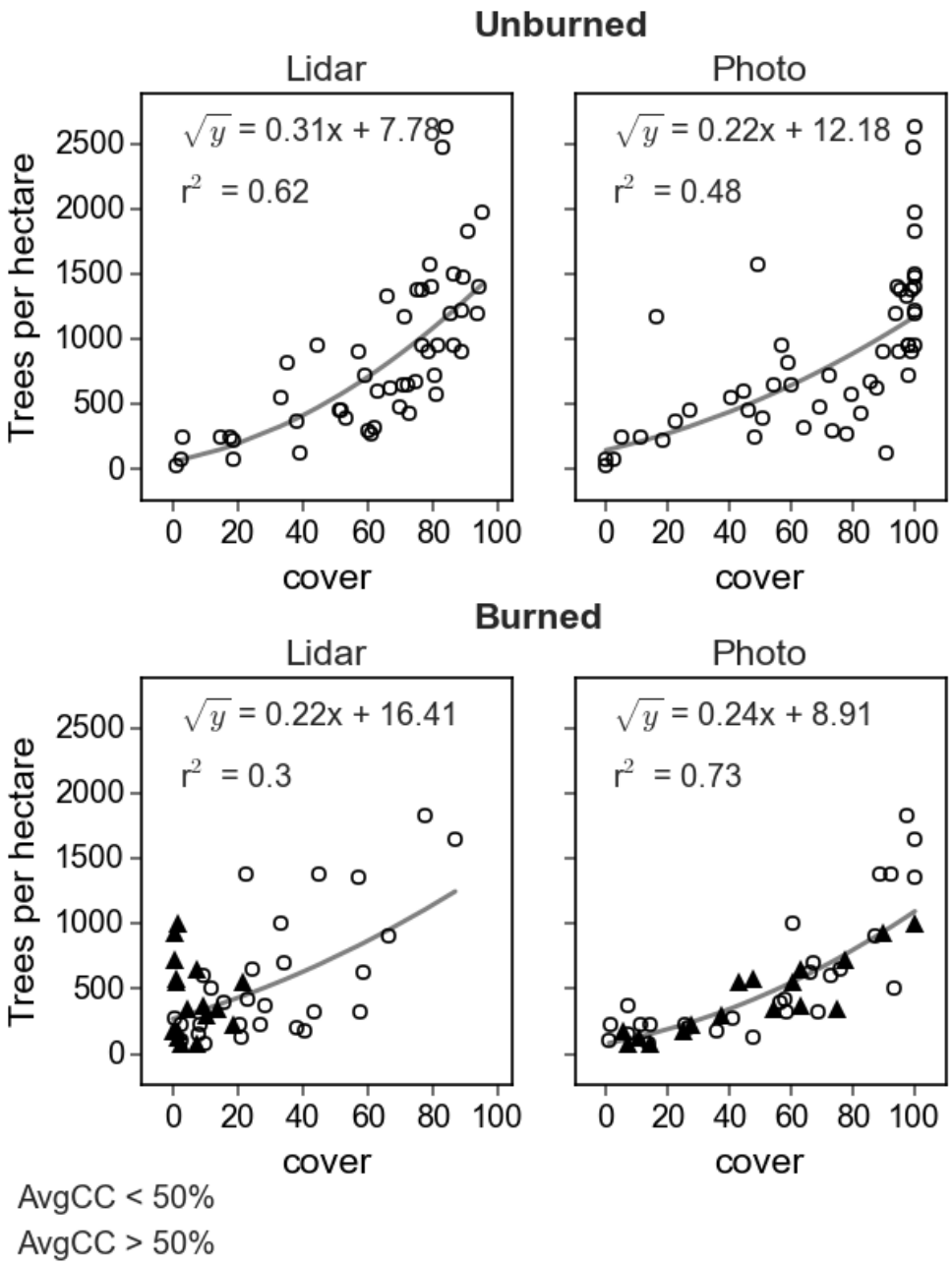

Figure 4. Scatterplots of the cover metric against field tree density for lidar and photogrammetry on unburned and burned plots with line of best fit (grey). For lidar, plots with greater than 50% average canopy consumption (black triangle) have low cover and high residuals even for plots with moderate to high tree density. All regressions were significant at the 0.05 level.

Table 4. Linear models of structure attributes with lidar metrics for all plots. Field estimated average crown consumption (AvgCC) was included as an independent variable and an interaction with the selected lidar metrics. Adjusted R^2 is also shown for models with and without incorporating AvgCC. P-values for each term are given as ns: $p > 0.05$, *: $p < 0.05$, **: $p < 0.01$.

Response	Model	Adj R^2 without AvgCC	Adj R^2 with AvgCC
HMAX	1.04^{ns} + 0.88 Hmax** + 0.05 AvgCC** - 0.003 Hmax:AvgCC*	0.82	0.84
HLOR	1.75* + 0.65 Hmax** + 0.03 AvgCC* - 0.002 Hmax:$AvgCC^{ns}$	0.74	0.75
BA	-8.79* + 3.22 p25** + 0.34 density** + 0.15 AvgCC* - 0.02 p25:$AvgCC^{ns}$ + 0.0 density:$AvgCC^{ns}$	0.65	0.66
AGB	-17.49^{ns} + 12.49 Havg** + 2.33 d02** + 0.46 $AvgCC^{ns}$ - 0.084 Havg:$AvgCC^{ns}$ + 0.023 d02:$AvgCC^{ns}$	0.64	0.64
CBD	-0.024^{ns} + 0.023 p25** - 0.004 $range^{ns}$ + 0.002 cover** + 0.001 $AvgCC^{ns}$ + 0.0 p25:$AvgCC^{ns}$ + 0.0 range:$AvgCC^{ns}$ + 0.0 cover:$AvgCC^{ns}$	0.46	0.47
CBH	1.97** + 0.37 p50** + 0.02 $d02^{ns}$ + 0.002 $AvgCC^{ns}$ - 0.001 p50:$AvgCC^{ns}$ + 0.001 d02:$AvgCC^{ns}$	0.64	0.65

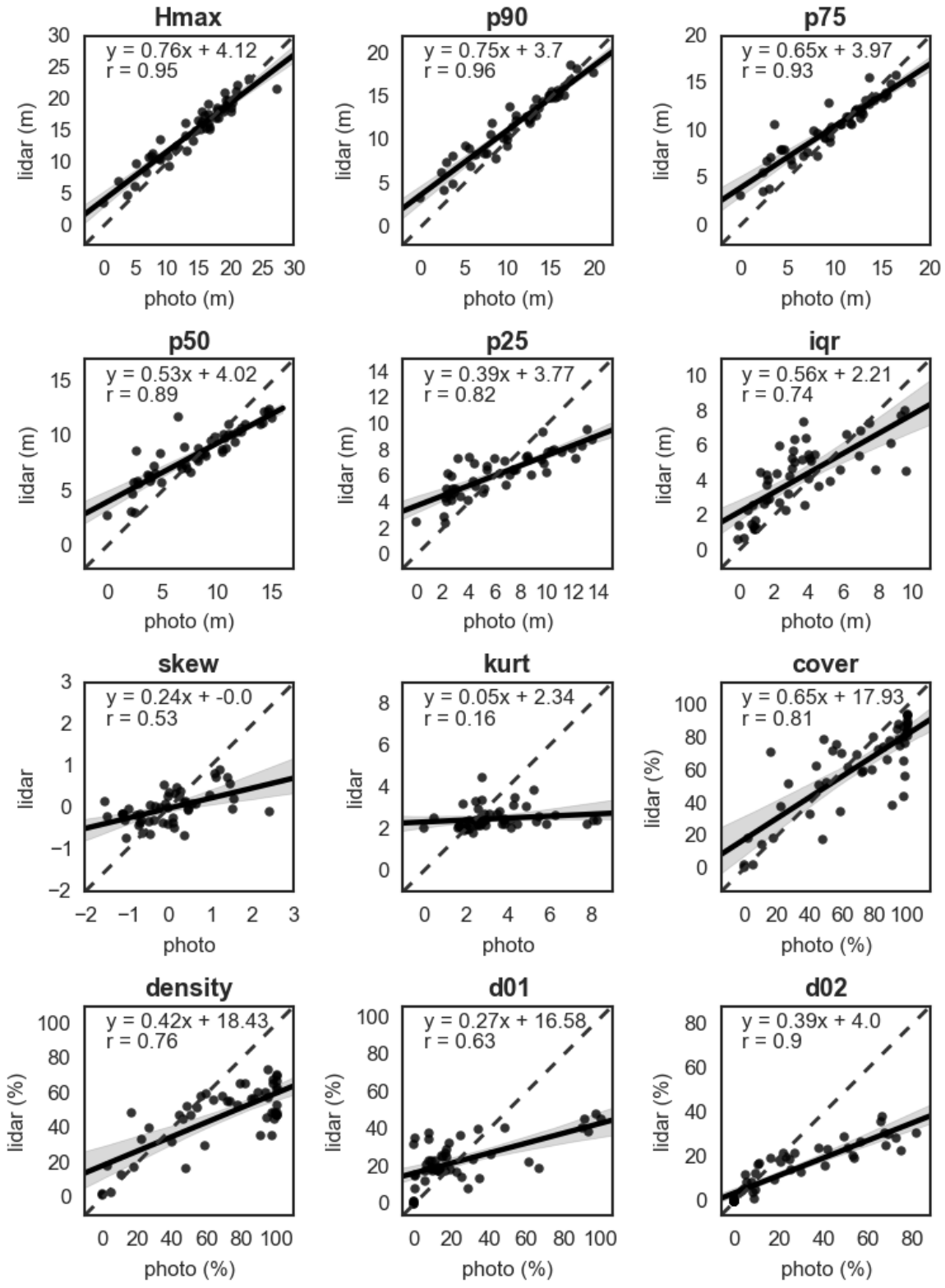

Figure 5. Scatterplots of corresponding point cloud metrics from lidar and photogrammetry for unburned plots with line of best fit (solid), one-to-one line (black dashed), and confidence intervals (grey). The linear model and Pearson product-moment correlation coefficient (r) are shown for each of the corresponding metrics.

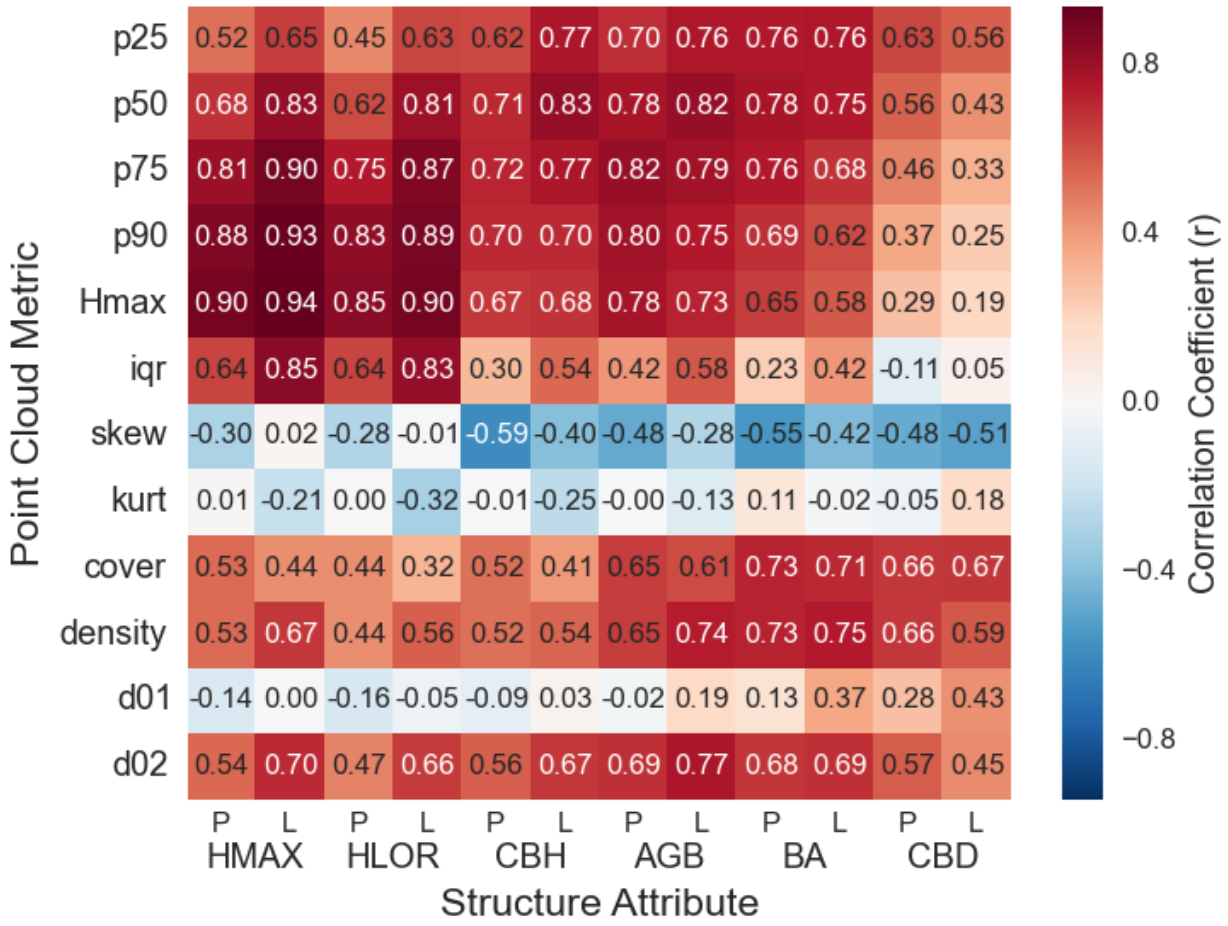

Figure 6. Heatmap of Pearson product-moment correlation coefficient (r) between select point cloud metrics for lidar (L) and photogrammetry (P) with forest structure attributes on unburned plots. Most lidar height metrics have higher correlations than photogrammetry with the height attributes HMAX, HLOR, and CBH. Lidar density metrics also tend to have higher correlations with the structure attributes than photogrammetry, but some photogrammetry height metrics show stronger correlations than lidar with AGB, BA, and CBD.

Table 5. Models of forest structure attributes with lidar and photogrammetry on **unburned** plots (a) and **burned** plots (b). RMSE is from leave-one-out cross-validation, and %RMSE expresses RMSE as a percent of the mean observed value. Photogrammetry estimated HMAX with higher accuracy when excluding a single plot that had several noise points above the tree canopy.

(a) Unburned Plots

Response	Dataset	N	Adj R^2	RMSE	%RMSE	Model
HMAX	photo	48	0.81	1.87	13.2	4.95 + 0.64 Hmax
	photo (no outlier)	*47*	*0.86*	*1.57*	*11.15*	*4.3 + 0.7 Hmax*
	lidar	48	0.88	1.43	10.1	1.69 + 0.83 Hmax
HLOR	photo	50	0.72	1.86	16.2	4.94 + 0.45 Hmax
	lidar	50	0.81	1.40	12.3	2.39 + 0.6 Hmax
BA	photo	50	0.65	7.58	27.7	3.43 + 1.96 Havg + 0.12 cover
	photo & texture	50	0.66	8.32	30.1	-7.15 + 2.3 Havg + 0.44 glcm_mean
	lidar	50	0.67	8.67	29.8	-9.23 + 3.62 p25 + 0.3 density
AGB	photo	50	0.68	38.08	31.0	18.18 + 9.44 p75 + 0.47 d02
	lidar	50	0.68	36.12	29.3	-20.52 + 14.69 p50 + 1.48 d02
CBD	photo	47	0.43	0.08	36.8	0.057 + 0.0023 cover
	photo & texture	47	0.45	0.09	41.6	-0.05 + 0.015 p25 + 0.0047 glcm_mean
	lidar	47	0.44	0.08	36.7	0.028 + 0.003 cover
CBH	photo	47	0.51	1.05	19.1	3.23 + 0.22 p75
	lidar	47	0.68	0.74	13.5	1.56 + 0.46 p50

(b) Burned Plots

Response	Dataset	N	Adj R^2	RMSE	%RMSE	Model
HMAX	photo	38	0.77	2.41	17.4	4.02 + 0.75 Hmax
	lidar	38	0.76	2.52	18.2	3.35 + 0.76 Hmax
HLOR	photo	45	0.78	2.05	18.8	5.89 + 2.04 stdev
	lidar	45	0.70	2.71	24.4	4.81 + 0.58 range
BA	photo	45	0.66	6.26	35.1	-1.01 + 1.68 Havg + 0.17 cover
	lidar	45	0.40	8.59	46.2	4.1 + 1.73 p25 + 0.82 d02
AGB	photo	45	0.59	34.36	41.9	-11.43 + 10.98 Havg + 0.48 cover
	lidar	45	0.50	36.86	45.0	10.81 + 3.96 Hmax + 3.84 d02
CBD	photo	39	0.64	0.09	56.3	-0.03 + 0.05 p10
	photo & texture	39	0.72	0.08	51.7	-0.08 + 0.04 p10 - 0.03 skew + 0.02 glcm_contrast
	lidar	39	0.48	0.09	59.5	-0.04 + 0.03 p10 + 0.01 d01
CBH	photo	39	0.63	0.82	17.8	2.09 + 0.31 p75
	lidar	39	0.64	0.80	17.6	2.2 + 0.21 p75 + 0.09 d02

Table 6. Models incorporating lidar and photogrammetry together for unburned plots which had low or insignificant slope and intercept bias when regressing by source. Source intercept and slope bias are the intercept and slope of including data source as a categorical variable in regressing the observed response on predicted values of the response. Source was significant in all models of HMAX and models of HLOR with high R^2 values, but the model with the maximum R^2 (shown below) had relatively low levels of bias.

					Intercept		Slope	
Response	N	R^2	%RMSE	Model	bias	p-value	bias	p-value
HMAX	96	0.83	11.7	3.69 + 0.72 Hmax	4.24	0.00	-0.27	0.00
HLOR	100	0.76	13.0	3.79 + 0.48 p90 + 0.14 range + 0.04 d00	3.00	0.03	-0.23	0.04
BA	100	0.61	28.6	0.01 + 1.14 p90 + 0.22 cover	8.47	0.08	-0.32	0.06
AGB	100	0.65	29.1	-34.69 + 13.63 p75 + 4.96 kur + 0.48 d00	34.64	0.09	-0.28	0.07
CBD	94	0.46	35.0	0.08 + 5e-4 Hqavg - 4e-3 range + 2e-3 cover	0.06	0.27	-0.38	0.12
CBH	94	0.59	14.7	1.54 + 0.31 p75 + 0.22 kurt + 0.01 d00	1.17	0.25	-0.24	0.18

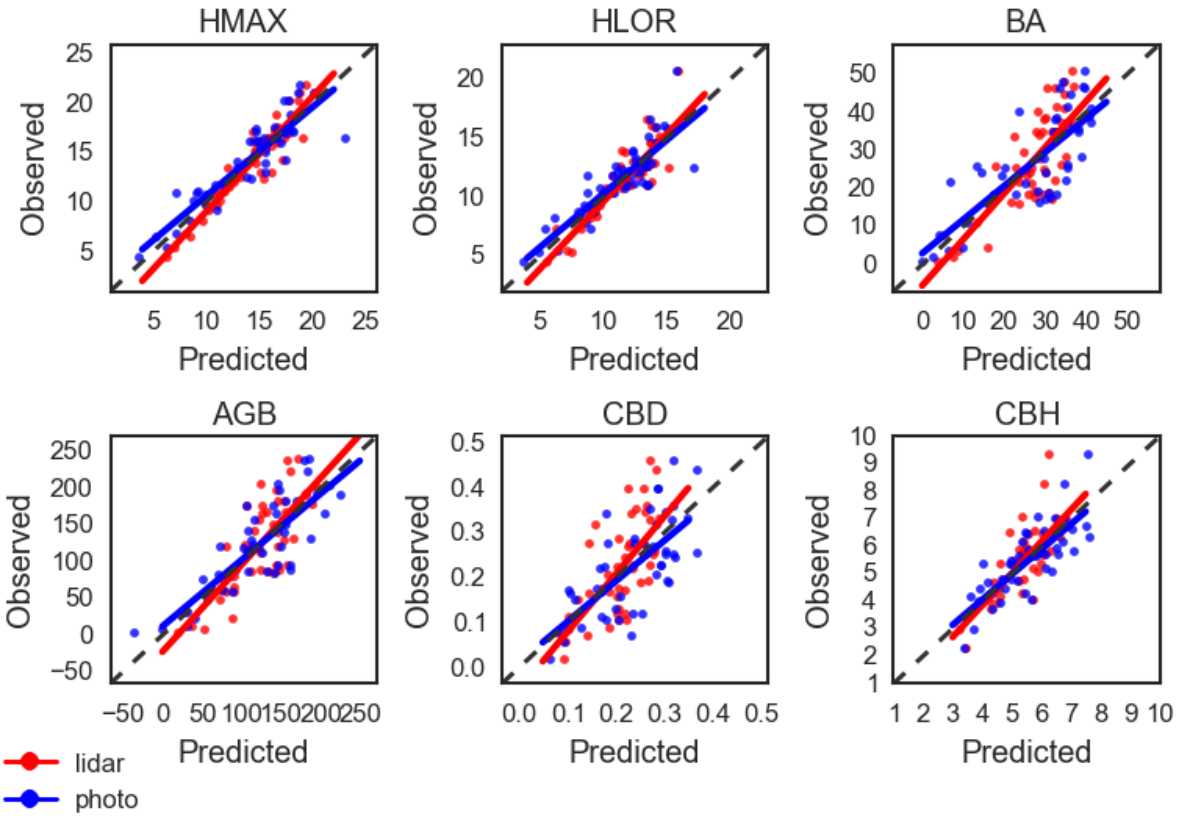

Figure 7. Observed against predicted values of forest structure attributes for models created with metrics combined from lidar and photogrammetry. Regression lines for lidar and photogrammetry have similar slopes and intercepts, showing that data source was an insignificant factor in modeling structure attributes.

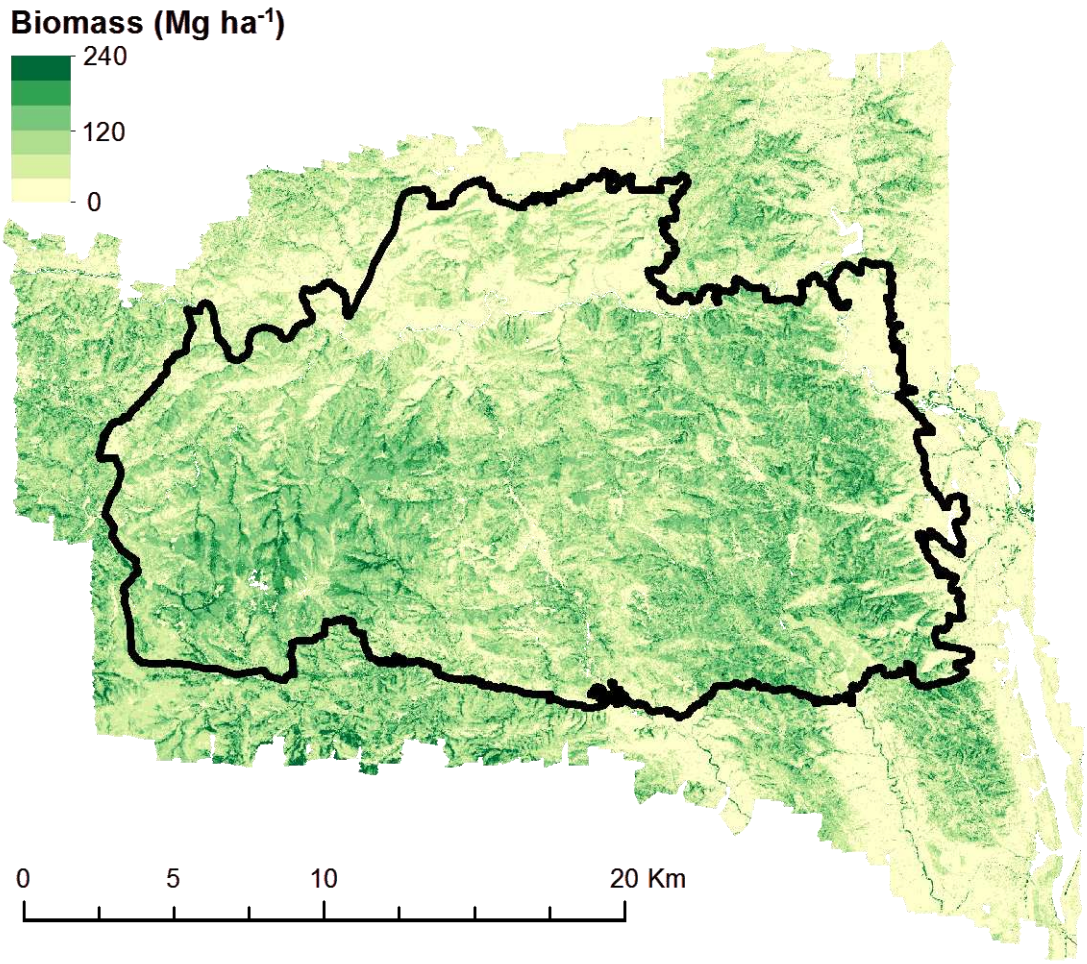

Figure 8. Map of pre-fire aboveground biomass from photogrammetry using the model calibrated on unburned plots. High levels of biomass are concentrated in drainages and on northern aspects in the eastern portion of the burn scar.

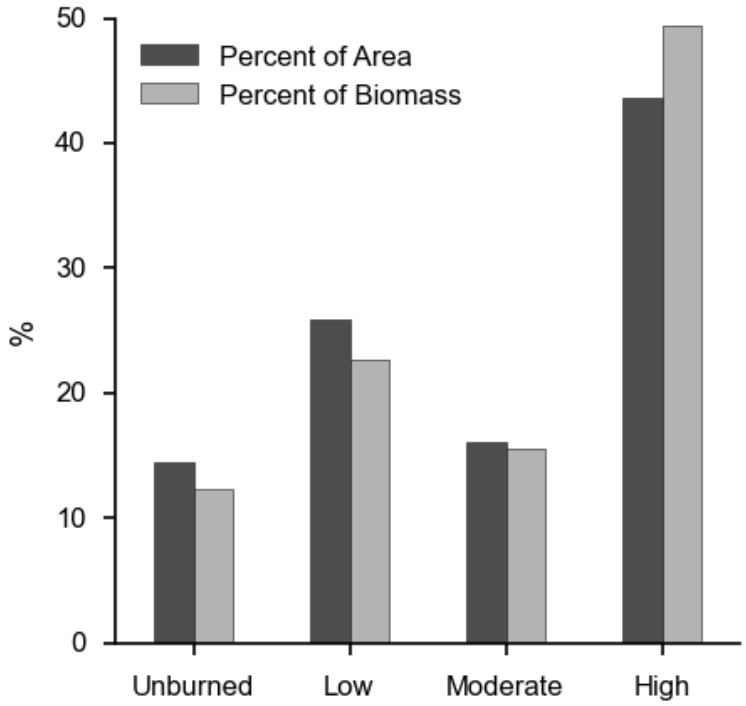

Figure 9. Percent of the total area and biomass within each burn severity.

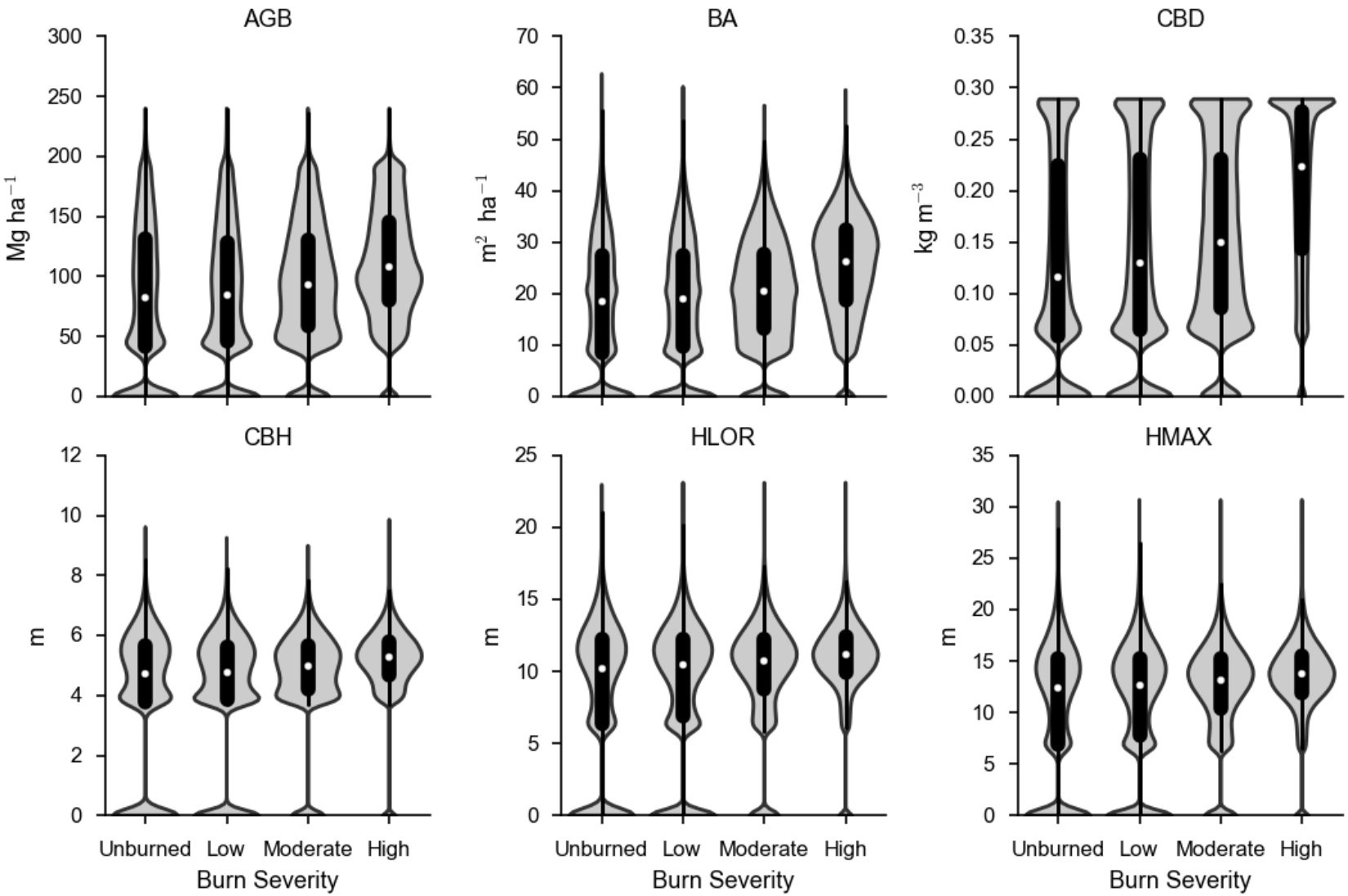

Figure 10. Violin plots of forest structure attributes by burn severity which show the kernel density estimate (grey) on top of the interquartile range (thick black line) and median (white circle). Except for slightly higher levels of AGB, BA, and CBD in high severity areas, forest structure was similar for all burn severities. The heavy zero loading in these distributions is due to the inclusion of unforested areas.

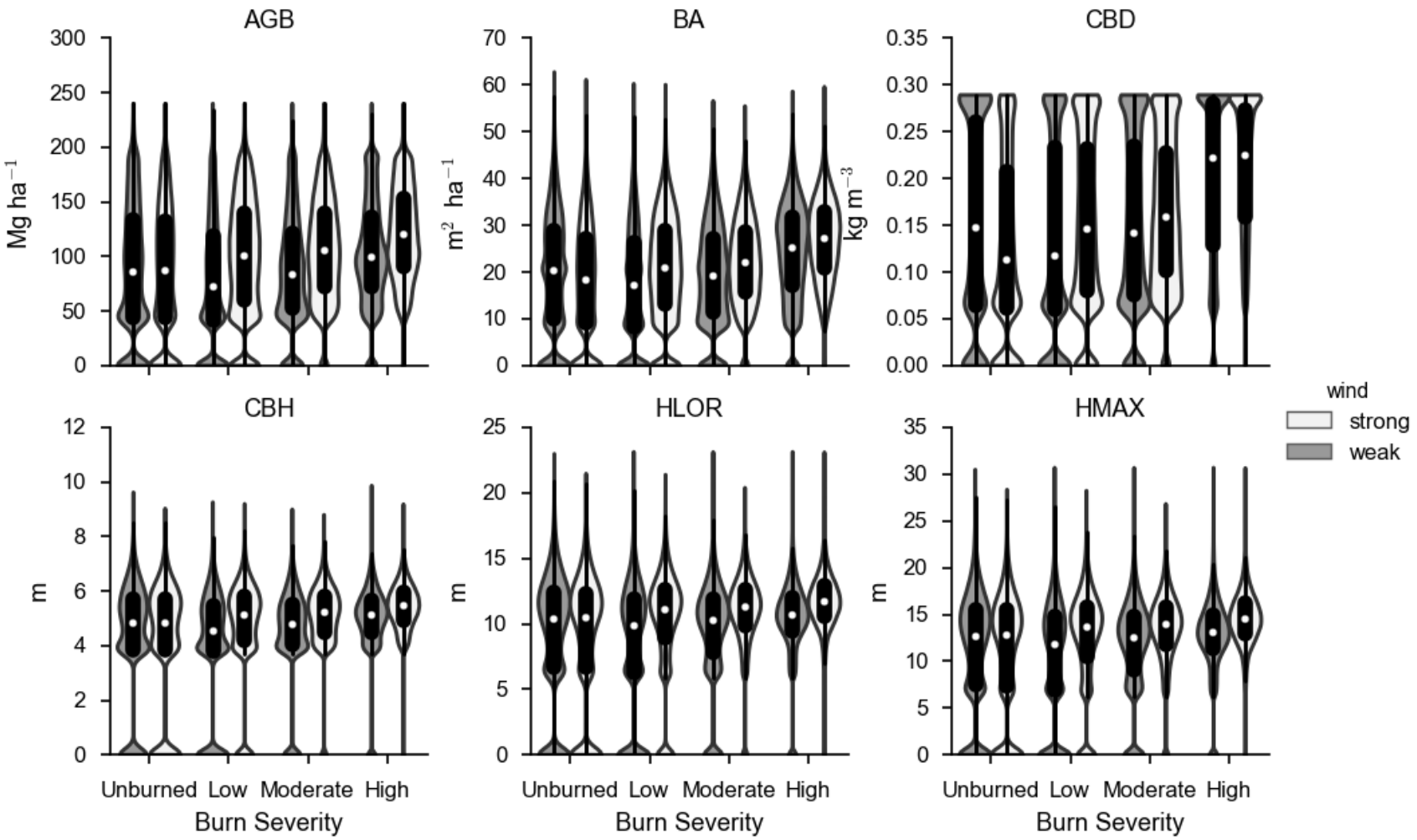

Figure 11. Violin plots of pre-fire forest structure by burn severity and weather conditions on the day an area was burned, which show the kernel density estimate on top of the interquartile range (thick black line) and median (white circle). The burn area expanded rapidly during the first two days of the fire when winds were strong and grew more slowly on the remaining 21 days. Forest structure appears similar across burn severities even when accounting for weather conditions on the day an area burned.

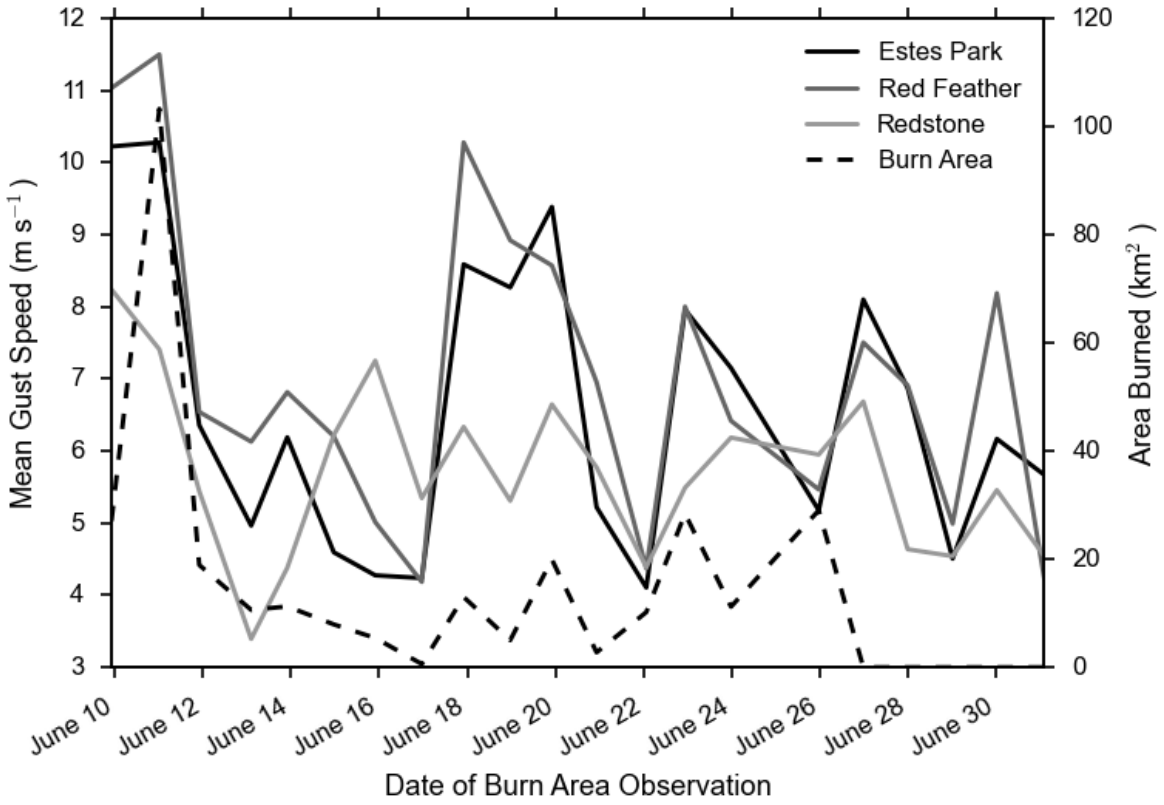

Figure 12. The area burned as measured by nightly thermal imaging corresponded with mean gust speed measured at three nearby RAWS stations over the previous day. The measurements for June 26th are for the previous two days because of a one day gap in the thermal imaging observations. Gust speed for June 10th was averaged from the first report of the fire on June 9th at 5:54 am to the first thermal imaging observation.

7 References

Alexander, J. D., Seavy, N. E., Ralph, C. J., & Hogoboom, B. (2006). Vegetation and topographical correlates of fire severity from two fires in the Klamath-Siskiyou region of Oregon and California. *International Journal of Wildland Fire*, *15*(2), 237–245.

Andersen, H.-E., McGaughey, R. J., & Reutebuch, S. E. (2005). Estimating forest canopy fuel parameters using LIDAR data. *Remote Sensing of Environment*, *94*(4), 441–449.

Andersen, H.-E., Reutebuch, S. E., & McGaughey, R. J. (2006). A rigorous assessment of tree height measurements obtained using airborne lidar and conventional field methods. *Canadian Journal of Remote Sensing*, *32*(5), 355–366.

Anderson, R. S., & Bolstad, P. V. (2013). Estimating Aboveground Biomass and Average Annual Wood Biomass Increment with Airborne Leaf-on and Leaf-off LiDAR in Great Lakes Forest Types. *Northern Journal of Applied Forestry*, *30*(1), 16–22. http://doi.org/10.5849/njaf.12-015

Axelsson, P. (2000). DEM generation from laser scanner data using adaptive TIN models. *International Archives of Photogrammetry and Remote Sensing*, *33*(B4/1; PART 4), 111–118.

Bigler, C., Kulakowski, D., & Veblen, T. T. (2005). Multiple Disturbance Interactions and Drought Influence Fire Severity in Rocky Mountain Subalpine Forests. *Ecology*, *86*(11), 3018–3029. http://doi.org/10.1890/05-0011

Bohlin, J., Wallerman, J., & Fransson, J. E. S. (2012). Forest variable estimation using photogrammetric matching of digital aerial images in combination with a high-resolution DEM. *Scandinavian Journal of Forest Research*, *27*(7), 692–699. http://doi.org/10.1080/02827581.2012.686625

Bolton, D. K., Coops, N. C., & Wulder, M. A. (2015). Characterizing residual structure and forest recovery following high-severity fire in the western boreal of Canada using Landsat time-series and airborne lidar data. *Remote Sensing of Environment*, *163*, 48–60. http://doi.org/10.1016/j.rse.2015.03.004

Broncano, M., & Retana, J. (2004). Topography and forest composition affecting the variability in fire severity and post-fire regeneration occurring after a large fire in the Mediterranean basin. *International Journal of Wildland Fire*, *13*(2), 209–216.

Campbell, J., Donato, D., Azuma, D., & Law, B. (2007). Pyrogenic carbon emission from a large wildfire in Oregon, United States. *Journal of Geophysical Research*, *112*(G4). http://doi.org/10.1029/2007JG000451

Carlson, T. N., & Ripley, D. A. (1997). On the relation between NDVI, fractional vegetation cover, and leaf area index. *Remote Sensing of Environment*, *62*(3), 241–252. http://doi.org/10.1016/S0034-4257(97)00104-1

Chasmer, L., Hopkinson, C., Smith, B., & Treitz, P. (2006). Examining the influence of changing laser pulse repetition frequencies on conifer forest canopy returns. *Photogrammetric Engineering & Remote Sensing*, *72*(12), 1359–1367.

Chojnacky, D. C., Heath, L. S., & Jenkins, J. C. (2014). Updated generalized biomass equations for North American tree species. *Forestry*, *87*(1), 129–151. http://doi.org/10.1093/forestry/cpt053

Coen, J. L., & Schroeder, W. (2015). The High Park fire: Coupled weather-wildland fire model simulation of a windstorm-driven wildfire in Colorado's Front Range: Simulation of windstorm-driven wildfire. *Journal of Geophysical Research: Atmospheres*, *120*(1), 131–146. http://doi.org/10.1002/2014JD021993

Colomina, I., & Molina, P. (2014). Unmanned aerial systems for photogrammetry and remote sensing: A review. *ISPRS Journal of Photogrammetry and Remote Sensing*, *92*, 79–97. http://doi.org/10.1016/j.isprsjprs.2014.02.013

Cruz, M. G., Alexander, M. E., & Wakimoto, R. H. (2003). Assessing canopy fuel stratum characteristics in crown fire prone fuel types of western North America. *International Journal of Wildland Fire*, *12*(1), 39–50.

Dubayah, R. O., & Drake, J. B. (2000). Lidar Remote Sensing for Forestry. *Journal of Forestry*, *98*(6), 44–46.

Erdody, T. L., & Moskal, L. M. (2010). Fusion of LiDAR and imagery for estimating forest canopy fuels. *Remote Sensing of Environment*, *114*(4), 725–737.

Farr, T. G., Rosen, P. A., Caro, E., Crippen, R., Duren, R., Hensley, S., … Alsdorf, D. (2007). The Shuttle Radar Topography Mission. *Reviews of Geophysics*, *45*(2). http://doi.org/10.1029/2005RG000183

Flannigan, M. D., Krawchuk, M. A., de Groot, W. J., Wotton, B. M., & Gowman, L. M. (2009). Implications of changing climate for global wildland fire. *International Journal of Wildland Fire*, *18*(5), 483–507.

Frolking, S., Palace, M. W., Clark, D. B., Chambers, J. Q., Shugart, H. H., & Hurtt, G. C. (2009). Forest disturbance and recovery: A general review in the context of spaceborne remote sensing of impacts on aboveground biomass and canopy structure. *Journal of Geophysical Research: Biogeosciences*, *114*(G2), n/a–n/a. http://doi.org/10.1029/2008JG000911

GeoMAC Wildfire Map. (2012). Geospatial Multi-Agency Coordination. Retrieved from http://www.geomac.gov/

Gobakken, T., Bollandsås, O. M., & Næsset, E. (2015). Comparing biophysical forest characteristics estimated from photogrammetric matching of aerial images and airborne laser scanning data. *Scandinavian Journal of Forest Research*, *30*(1), 73–86. http://doi.org/10.1080/02827581.2014.961954

Goetz, S. J., & Dubayah, R. (2011). Advances in remote sensing technology and implications for measuring and monitoring forest carbon stocks and change. *Carbon Management*, *2*(3), 231–244. http://doi.org/10.4155/cmt.11.18

Goetz, S. J., Sun, M., Baccini, A., & Beck, P. S. A. (2010). Synergistic use of spaceborne lidar and optical imagery for assessing forest disturbance: An Alaska case study. *Journal of Geophysical Research: Biogeosciences*, *115*(G2), G00E07. http://doi.org/10.1029/2008JG000898

Greene, D. F., & Johnson, E. A. (1999). Modelling recruitment of Populus tremuloides, Pinus banksiana, and Picea mariana following fire in the mixedwood boreal forest. *Canadian Journal of Forest Research*, *29*(4), 462–473. http://doi.org/10.1139/x98-211

Gruen, A. (2012). Development and Status of Image Matching in Photogrammetry. *The Photogrammetric Record*, *27*(137), 36–57. http://doi.org/10.1111/j.1477-9730.2011.00671.x

Hall, S. A., Burke, I. C., Box, D. O., Kaufmann, M. R., & Stoker, J. M. (2005). Estimating stand structure using discrete-return lidar: an example from low density, fire prone ponderosa pine forests. *Forest Ecology and Management*, *208*(1–3), 189–209. http://doi.org/10.1016/j.foreco.2004.12.001

Haralick, R. M., Shanmugam, K., & Dinstein, I. H. (1973). Textural features for image classification. *Systems, Man and Cybernetics, IEEE Transactions on*, (6), 610–621.

Harvey, B. J., Donato, D. C., Romme, W. H., & Turner, M. G. (2013). Influence of recent bark beetle outbreak on fire severity and postfire tree regeneration in montane Douglas-fir forests. *Ecology*, *94*(11), 2475–2486. http://doi.org/10.1890/13-0188.1

Hermosilla, T., Ruiz, L. A., Kazakova, A. N., Coops, N. C., & Moskal, L. M. (2014). Estimation of forest structure and canopy fuel parameters from small-footprint full-waveform LiDAR data. *International Journal of Wildland Fire*. Retrieved from http://dx.doi.org/10.1071/WF13086

Hernández-Stefanoni, J. L., Johnson, K. D., Cook, B. D., Dupuy, J. M., Birdsey, R., Peduzzi, A., & Tun-Dzul, F. (2015). Estimating species richness and biomass of tropical dry forests using LIDAR during leaf-on and leaf-off canopy conditions. *Applied Vegetation Science*, *18*(4), 724–732. http://doi.org/10.1111/avsc.12190

Hirschmuller, H. (2008). Stereo Processing by Semiglobal Matching and Mutual Information. *IEEE Transactions on Pattern Analysis and Machine Intelligence*, *30*(2), 328–341. http://doi.org/10.1109/TPAMI.2007.1166

Hudak, A. T., & Wessman, C. A. (1998). Textural analysis of historical aerial photography to characterize woody plant encroachment in South African savanna. *Remote Sensing of Environment*, *66*(3), 317–330.

Isenburg, M. (2011). LAStools - efficient tools for LiDAR processing (Version 130506). Retrieved from http://lastools.org

Järnstedt, J., Pekkarinen, A., Tuominen, S., Ginzler, C., Holopainen, M., & Viitala, R. (2012). Forest variable estimation using a high-resolution digital surface model. *ISPRS Journal of Photogrammetry and Remote Sensing*, *74*, 78–84. http://doi.org/10.1016/j.isprsjprs.2012.08.006

Jenkins, J. C., Chojnacky, D. C., Heath, L. S., & Birdsey, R. A. (2003). National-scale biomass estimators for United States tree species. *Forest Science*, *49*(1), 12–35.

Johnson, D. W., Murphy, J. F., Susfalk, R. B., Caldwell, T. G., Miller, W. W., Walker, R. F., & Powers, R. F. (2005). The effects of wildfire, salvage logging, and post-fire N-fixation on the nutrient budgets of a Sierran forest. *Forest Ecology and Management*, *220*(1–3), 155–165. http://doi.org/10.1016/j.foreco.2005.08.011

Kane, V. R., Cansler, C. A., Povak, N. A., Kane, J. T., McGaughey, R. J., Lutz, J. A., … North, M. P. (2015). Mixed severity fire effects within the Rim fire: Relative importance of local climate, fire weather, topography, and forest structure. *Forest Ecology and Management*, *358*, 62–79. http://doi.org/10.1016/j.foreco.2015.09.001

Kane, V. R., North, M. P., Lutz, J. A., Churchill, D. J., Roberts, S. L., Smith, D. F., … Brooks, M. L. (2013). Assessing fire effects on forest spatial structure using a fusion of Landsat and airborne LiDAR

data in Yosemite National Park. *Remote Sensing of Environment*. http://doi.org/10.1016/j.rse.2013.07.041

Kaufmann, M. R., Stoker, J. M., & Greenlee, S. K. (2006). *Using Lidar to identify sediment and forest structure change in the Hayman burn, Colorado* (Joint Fire Sciences Program Project No. 03-2-3-18) (p. 11). Retrieved from http://www.firescience.gov/projects/03-2-3-18/project/03-2-3-18_final_report.pdf

Keane, R. E. (2015). Fuel Mapping. In *Wildland Fuel Fundamentals and Applications* (pp. 153–174). Springer International Publishing. Retrieved from http://link.springer.com/10.1007/978-3-319-09015-3

Keyser, C. E., & Dixon, G. E. (2015, November 2). Central Rockies (CR) Variant Overview - Forest Vegetation Simulator [Software Manual]. USDA, Forest Service, Forest Management Service Center. Retrieved from http://www.fs.fed.us/fmsc/ftp/fvs/docs/overviews/FVScr_Overview.pdf

Korhonen, L., Korpela, I., Heiskanen, J., & Maltamo, M. (2011). Airborne discrete-return LIDAR data in the estimation of vertical canopy cover, angular canopy closure and leaf area index. *Remote Sensing of Environment*, *115*(4), 1065–1080. http://doi.org/10.1016/j.rse.2010.12.011

Kuhn, M., & Johnson, K. (2013). *Applied Predictive Modeling*. New York, NY: Springer New York. Retrieved from http://link.springer.com/10.1007/978-1-4614-6849-3

Lefsky, M. A., Cohen, W. B., Parker, G. G., & Harding, D. J. (2002). Lidar Remote Sensing for Ecosystem Studies. *BioScience*, *52*(1), 19. http://doi.org/10.1641/0006-3568(2002)052[0019:LRSFES]2.0.CO;2

Lefsky, M. A., Turner, D. P., Guzy, M., & Cohen, W. B. (2005). Combining lidar estimates of aboveground biomass and Landsat estimates of stand age for spatially extensive validation of modeled forest productivity. *Remote Sensing of Environment*, *95*(4), 549–558. http://doi.org/10.1016/j.rse.2004.12.022

Lentile, L. B., Holden, Z. A., Smith, A. M. S., Falkowski, M. J., Hudak, A. T., Morgan, P., … Benson, N. C. (2006). Remote sensing techniques to assess active fire characteristics and post-fire effects. *International Journal of Wildland Fire*, *15*(3), 319–345.

Lentile, L. B., Smith, F. W., & Shepperd, W. D. (2006). Influence of topography and forest structure on patterns of mixed severity fire in ponderosa pine forests of the South Dakota Black Hills, USA. *International Journal of Wildland Fire*, *15*(4), 557. http://doi.org/10.1071/WF05096

Lydersen, J. M., North, M. P., & Collins, B. M. (2014). Severity of an uncharacteristically large wildfire, the Rim Fire, in forests with relatively restored frequent fire regimes. *Forest Ecology and Management*, *328*, 326–334. http://doi.org/10.1016/j.foreco.2014.06.005

Maltamo, M., Næsset, E., & Vauhkonen, J. (Eds.). (2014). *Forestry Applications of Airborne Laser Scanning* (Vol. 27). Dordrecht: Springer Netherlands. Retrieved from http://link.springer.com/10.1007/978-94-017-8663-8

Mehtatalo, L. (2015). lmfor: Functions for Forest Biometrics (Version 1.1). Retrieved from http://CRAN.R-project.org/package=lmfor

Meigs, G. W., Donato, D. C., Campbell, J. L., Martin, J. G., & Law, B. E. (2009). Forest Fire Impacts on Carbon Uptake, Storage, and Emission: The Role of Burn Severity in the Eastern Cascades, Oregon. *Ecosystems*, *12*(8), 1246–1267. http://doi.org/10.1007/s10021-009-9285-x

Michalek, J. L., French, N. H. F., Kasischke, E. S., Johnson, R. D., & Colwell, J. E. (2000). Using Landsat TM data to estimate carbon release from burned biomass in an Alaskan spruce forest complex. *International Journal of Remote Sensing*, *21*(2), 323–338. http://doi.org/10.1080/014311600210858

Montesano, P. M., Sun, G., Dubayah, R., & Ranson, K. J. (2014). The Uncertainty of Plot-Scale Forest Height Estimates from Complementary Spaceborne Observations in the Taiga-Tundra Ecotone. *Remote Sensing*, *6*(10), 10070–10088. http://doi.org/10.3390/rs61010070

Næsset, E. (2002). Predicting forest stand characteristics with airborne scanning laser using a practical two-stage procedure and field data. *Remote Sensing of Environment*, *80*(1), 88–99. http://doi.org/10.1016/S0034-4257(01)00290-5

Næsset, E. (2005). Assessing sensor effects and effects of leaf-off and leaf-on canopy conditions on biophysical stand properties derived from small-footprint airborne laser data. *Remote Sensing of Environment*, *98*(2–3), 356–370. http://doi.org/10.1016/j.rse.2005.07.012

Nappi, A., & Drapeau, P. (2011). Pre-fire forest conditions and fire severity as determinants of the quality of burned forests for deadwood-dependent species: the case of the black-backed woodpecker. *Canadian Journal of Forest Research*, *41*(5), 994–1003. http://doi.org/10.1139/x11-028

Natural Resources Conservation Service, Larimer County, United States Forest Service, & Colorado Department of Transportation. (2012). *High Park Fire Burned Area Emergency Response Report*.

Nurminen, K., Karjalainen, M., Yu, X., Hyyppä, J., & Honkavaara, E. (2013). Performance of dense digital surface models based on image matching in the estimation of plot-level forest variables. *ISPRS Journal of Photogrammetry and Remote Sensing*, *83*, 104–115. http://doi.org/10.1016/j.isprsjprs.2013.06.005

Odion, D. C., Frost, E. J., Strittholt, J. R., Jiang, H., Dellasala, D. A., & Moritz, M. A. (2004). Patterns of Fire Severity and Forest Conditions in the Western Klamath Mountains, California. *Conservation Biology*, *18*(4), 927–936. http://doi.org/10.1111/j.1523-1739.2004.00493.x

Pearson, J. A., Fahey, T. J., & Knight, D. H. (1984). Biomass and leaf area in contrasting lodgepole pine forests. *Canadian Journal of Forest Research*, *14*(2), 259–265. http://doi.org/10.1139/x84-050

Photoscan Professional Edition. (2015). (Version 1.1.5). Agisoft LLC. Retrieved from http://www.agisoft.com/downloads/installer/

Pitt, D. G., Woods, M., & Penner, M. (2014). A Comparison of Point Clouds Derived from Stereo Imagery and Airborne Laser Scanning for the Area-Based Estimation of Forest Inventory Attributes in

Boreal Ontario. *Canadian Journal of Remote Sensing*, *40*(3), 214–232. http://doi.org/10.1080/07038992.2014.958420

Reeves, M. C., Ryan, K. C., Rollins, M. G., & Thompson, T. G. (2009). Spatial fuel data products of the LANDFIRE project. *International Journal of Wildland Fire*, *18*(3), 250–267.

Riegler, G., Hennig, S. D., & Weber, M. (2015). WORLDDEM – A NOVEL GLOBAL FOUNDATION LAYER. *ISPRS - International Archives of the Photogrammetry, Remote Sensing and Spatial Information Sciences*, *XL-3/W2*, 183–187. http://doi.org/10.5194/isprsarchives-XL-3-W2-183-2015

Rodriguez, E., & Martin, J. M. (1992). Theory and design of interferometric synthetic aperture radars. In *Radar and Signal Processing, IEE Proceedings F* (Vol. 139, pp. 147–159). IET. Retrieved from http://ieeexplore.ieee.org/xpls/abs_all.jsp?arnumber=136293

Schoennagel, T., Veblen, T. T., & Romme, W. H. (2004). The interaction of fire, fuels, and climate across Rocky Mountain forests. *BioScience*, *54*(7), 661–676.

Stone, B. H. (2015). *Mapping Burn Severity, Pine Beetle Infestation, and Their Interaction at the High Park Fire*. Colorado State University. Libraries. Retrieved from https://dspace.library.colostate.edu/handle/10217/167258

St-Onge, B., Hu, Y., & Vega, C. (2008). Mapping the height and above-ground biomass of a mixed forest using lidar and stereo Ikonos images. *International Journal of Remote Sensing*, *29*(5), 1277–1294. http://doi.org/10.1080/01431160701736505

Tadono, T., Ishida, H., Oda, F., Naito, S., Minakawa, K., & Iwamoto, H. (2014). Precise Global DEM Generation by ALOS PRISM. *ISPRS Annals of Photogrammetry, Remote Sensing and Spatial Information Sciences*, *II-4*, 71–76. http://doi.org/10.5194/isprsannals-II-4-71-2014

Thompson, J. R., & Spies, T. A. (2009). Vegetation and weather explain variation in crown damage within a large mixed-severity wildfire. *Forest Ecology and Management*, *258*(7), 1684–1694. http://doi.org/10.1016/j.foreco.2009.07.031

Tuominen, S., & Pekkarinen, A. (2005). Performance of different spectral and textural aerial photograph features in multi-source forest inventory. *Remote Sensing of Environment*, *94*(2), 256–268. http://doi.org/10.1016/j.rse.2004.10.001

Turner, M. G., Romme, W. H., & Gardner, R. H. (1999). Prefire heterogeneity, fire severity, and early postfire plant reestablishment in subalpine forests of Yellowstone National Park, Wyoming. *International Journal of Wildland Fire*, *9*(1), 21–36.

US EPA. (2014, April). Greenhouse Gas Equivalencies Calculator [Data and Tools]. Retrieved December 29, 2015, from http://www.epa.gov/energy/greenhouse-gas-equivalencies-calculator

van der Werf, G. R., Randerson, J. T., Giglio, L., Collatz, G. J., Mu, M., Kasibhatla, P. S., … van Leeuwen, T. T. (2010). Global fire emissions and the contribution of deforestation, savanna, forest, agricultural, and peat fires (1997–2009). *Atmospheric Chemistry and Physics*, *10*(23), 11707–11735. http://doi.org/10.5194/acp-10-11707-2010

Vastaranta, M., Wulder, M. A., White, J. C., Pekkarinen, A., Tuominen, S., Ginzler, C., … Hyyppä, H. (2013). Airborne laser scanning and digital stereo imagery measures of forest structure: comparative results and implications to forest mapping and inventory update. *Canadian Journal of Remote Sensing*, *39*(05), 382–395. http://doi.org/10.5589/m13-046

Véga, C., & St-Onge, B. (2008). Height growth reconstruction of a boreal forest canopy over a period of 58 years using a combination of photogrammetric and lidar models. *Remote Sensing of Environment*, *112*(4), 1784–1794. http://doi.org/10.1016/j.rse.2007.09.002

Vierling, K. T., Vierling, L. A., Gould, W. A., Martinuzzi, S., & Clawges, R. M. (2008). Lidar: shedding new light on habitat characterization and modeling. *Frontiers in Ecology and the Environment*, *6*(2), 90–98.

Wasser, L., Day, R., Chasmer, L., & Taylor, A. (2013). Influence of Vegetation Structure on Lidar-derived Canopy Height and Fractional Cover in Forested Riparian Buffers During Leaf-Off and Leaf-On Conditions. *PLoS ONE*, *8*(1), e54776. http://doi.org/10.1371/journal.pone.0054776

Westerling, A. L., Hidalgo, H. G., Cayan, D. R., & Swetnam, T. W. (2006). Warming and Earlier Spring Increase Western U.S. Forest Wildfire Activity. *Science*, *313*(5789), 940–943. http://doi.org/10.1126/science.1128834

White, J. C., Wulder, M. A., Vastaranta, M., Coops, N., Pitt, D., & Woods, M. (2013). The Utility of Image-Based Point Clouds for Forest Inventory: A Comparison with Airborne Laser Scanning. *Forests*, *4*(3), 518–536. http://doi.org/10.3390/f4030518

White, R. A., & Dietterick, B. C. (2012). Use of LiDAR and multispectral imagery to determine conifer mortality and burn severity following the lockheed fire (Vol. Gen. Tech. Rep. PSW-GTR-238, pp. 667–675). Presented at the Proceedings of Coast Redwood Forests in a Changing California: A Symposium for Scientists and Managers., Albany, CA: Pacific Southwest Research Station, Forest Service, US Department of Agriculture. Retrieved from http://www.fs.fed.us/psw/publications/documents/psw_gtr238/psw_gtr238_667.pdf

Wing, M. G., Eklund, A., & Sessions, J. (2010). Applying LiDAR technology for tree measurements in burned landscapes. *International Journal of Wildland Fire*, *19*(1), 104–114.

Wulder, M. A., White, J. C., Alvarez, F., Han, T., Rogan, J., & Hawkes, B. (2009). Characterizing boreal forest wildfire with multi-temporal Landsat and LIDAR data. *Remote Sensing of Environment*, *113*(7), 1540–1555. http://doi.org/10.1016/j.rse.2009.03.004

Wykoff, W. R., Crookston, N. L., & Stage, A. R. (1982). *User's guide to the stand prognosis model* (No. Gen. Tech. Rep. INT-133) (p. 112). Ogden, UT: U.S. Department of Agriculture, Forest Service, Intermountain Forest and Range Experiment Station. Retrieved from http://www.fs.fed.us/rm/pubs_int/int_gtr133.pdf

Yu, A. W., Krainak, M. A., Abshire, J. B., Cavanaugh, J., Valett, S., & Ramos-Izquierdo, L. (2010). Airborne Lidar Simulator for the Lidar Surface Topography (LIST) Mission. Presented at the 25th International Laser Radar Conference, St.Petersburg, Russia, Russia. Retrieved from http://ntrs.nasa.gov/search.jsp?R=20100019566

Zolkos, S. G., Goetz, S. J., & Dubayah, R. (2013). A meta-analysis of terrestrial aboveground biomass estimation using lidar remote sensing. *Remote Sensing of Environment*, *128*, 289–298. http://doi.org/10.1016/j.rse.2012.10.017